Multi-Ultrasonic Sensor Fusion for Mobile Robots in Confined Spaces

Zou Yi

School of Electrical & Electronic Engineering

A thesis submitted to the Nanyang Technological University
in fulfillment of the requirement for the degree of
Master of Engineering

2001

Statement of Originality

I hereby certify that the work embodied in this thesis is the result of original research done by me and has not been submitted for a higher degree to any other University or Institute.

....

Date Zou Yi

Acknowledgment

First and foremost, this work will never have gone this far if it has not been for the insightful guidance, valuable suggestions, timely encouragement and friendship, from my supervisor, Assoc Prof. Ho Yeong Khing. Without his continuous and extensive support, I will never be able to complete this project.

I would like to extend my special thanks to my co-supervisor Asst Prof. Chua Chin Seng, for his valuable comments on my project. Discussions with him have always been filled with inspirations and stimulations.

My personal thanks are also dedicated to all staff and colleagues in the Mechanical & Electrical Workshop, Instrumentation & System Engineering Lab, First Year Lab., for their continuous support during the period of my research. Special thanks to Mr. Zhou Xiao Wei, Mr. Chia Chiu Kiat, Mr. Tan Chai Soon and Mr. Yock Ching Fong, for their friendship and for always being fun to work with.

I also would like to extend my personal appreciations to the School of Electrical and Electronic Engineering of Nanyang Technological University, for the scholarship they provided so that I can concentrate on my research.

Last but not least, I wish to express my sincere thanks to my father, my mother and my brother, for sharing all my pains and joys, for encouraging and supporting me all the time.

Summary

In this work, issues pertaining to the multi-ultrasonic sensor fusion for the navigation of a sonar based mobile robot in confined spaces are investigated. Problems associated with multi-ultrasonic sensor fusion, such as those arising from specular reflections in confined environments, as well as the suitable framework for sensory information integration, have been studied. In particular, application of evidence grids as the sensor fusion framework is accomplished. Novel methods are introduced to deal with specular reflections. Experiments on the application of the range confidence factor have been done to test its effectiveness in reducing unreliable sonar responses. To make it work more intelligent in dealing with the specular reflections, we have exploited the use of the conflict value in Dempster-Shafer's evidence theory to build an adaptive sensor model. The new model would be able to adjust the parameters of the range confidence factor to better reduce the unreliable sonar readings. To further reduce the errors caused by specular reflections and other uncertainties in ultrasonic sensor responses, a new algorithm, the outlier rejection algorithm is also implemented. Experiments show that the evidence map obtained with the adaptive sensor model and outlier rejection algorithm is improved greatly.

Dead-reckoning error correction algorithms have been derived especially for our testing mobile robot platform to meet the need of the localization in navigation. Af-

ter dead reckoning errors have been compensated, based on the grid map produced, a simple path planning strategy has been developed to search for the empty areas in the surroundings of the robot. The path planning strategy produces the route that leads the robot for a safe navigation.

Contents

List of Figures

List of Tables

This work is dedicated to my family,
who always give me love and support.

Chapter 1

Introduction

1.1 Motivation

Development of service robots has always attracted much attention in the research community. Service robots should be able to perform "not-too-complicated" tasks reliably with low costs in environments such as offices, kitchens or toilets. The attempt to develop such robots has raised questions about how this type of robots should be built. To perform certain tasks in an unknown environment autonomously, the environment map is necessary for the control and the navigation of the robot [28, 43]. The autonomy of robot is based on the sensing of its environment and the interpretation of the sensory information [34, 35, 61]. This project is tasked with investigating some of the important aspects such as map building and autonomous navigation in a service robot for operating in a confined space. We have chosen to use ultrasonic sensors to achieve map building for the service robot in consideration of costs. The autonomous navigation of a multi-ultrasonic based mobile robot in an unknown confined environment has some challenging issues. The attempt to

provide solutions to these issues is what has motivated us in the project. Some of the challenging issues to be tackled are:

1. In order to build an accurate map, multi-sensory information must be integrated in an appropriate way. The robot would be able to know its surroundings properly if the multi-sensory information can be well integrated. Sensor fusion is a process of combining the multi-sensory data [57, 18, 74, 6, 62]. Fused multi-sensory data bring more information to the robot [43, 30, 58]. They provide complementary environmental information which enables the robot to act intelligently and robustly [74]. Some of the sensor fusion methods commonly used are Kalman filtering [12, 76], neural networks [13], Bayesian theory [4, 59, 26, 19] and Dempster-Shafer's [46, 79, 16] evidence theory. In our case, what methodology should be used for sensor fusion? How should the algorithm be implemented?

2. Using ultrasonic sensors in a confined environment has its own problems [43, 58], of which the most serious one is that arising from specular reflections [60, 42, 36]. How should one deal with theses problems? A sensor model is needed to convert the raw sensory information to a framework on which sensor fusion can be achieved. What ultrasonic sensor model should be used for the purpose of sensor fusion ? How would one develop a robust and intelligent ultrasonic sensor model is thus of great importance.

3. To update the map, the robot has to know its current position or states. This requires an effective localization algorithm [50, 10, 48]. Dead reckoning is a simple and easy approach [9, 27]. However, due to errors accumulated in the course of navigation [35], compensation is required to correct dead reckoning errors for better positional information. Concerning circumstances

in the navigation of our robot, how would one derive algorithms to compensate for the dead reckoning errors?

4. Path planning strategy [2, 36, 37, 38] should be considered in accordance to the task the robot is expected to perform. The service robot in this project is designed to clean the floor. Based on this, the path planning strategy should enable the robot to cover as much empty area as possible, without bumping into any obstacles. How should one develop a simple path planning algorithm to meet this purpose?

1.2 Objectives

Figure 1.1 shows the block diagram of the various modules constituting the main functional blocks for the autonomous navigation of our proposed service robot. These include the multi-ultrasonic sensor fusion, the grid-based map building, the dead reckoning error correction for localization and the path planning. With this proposed system design, the main objectives for this project include the following.

1. To apply the evidence theory for the purpose of multi-ultrasonic sensor fusion.
2. To apply the evidence grids as the framework for multi-ultrasonic sensor fusion.
3. To build the grid-based map from the integrated sensor information.
4. To analyze the specular reflections in confined spaces and reduce unreliable readings caused by these specular reflections.
5. To implement algorithms to compensate for the dead reckoning errors for better localization of the robot.

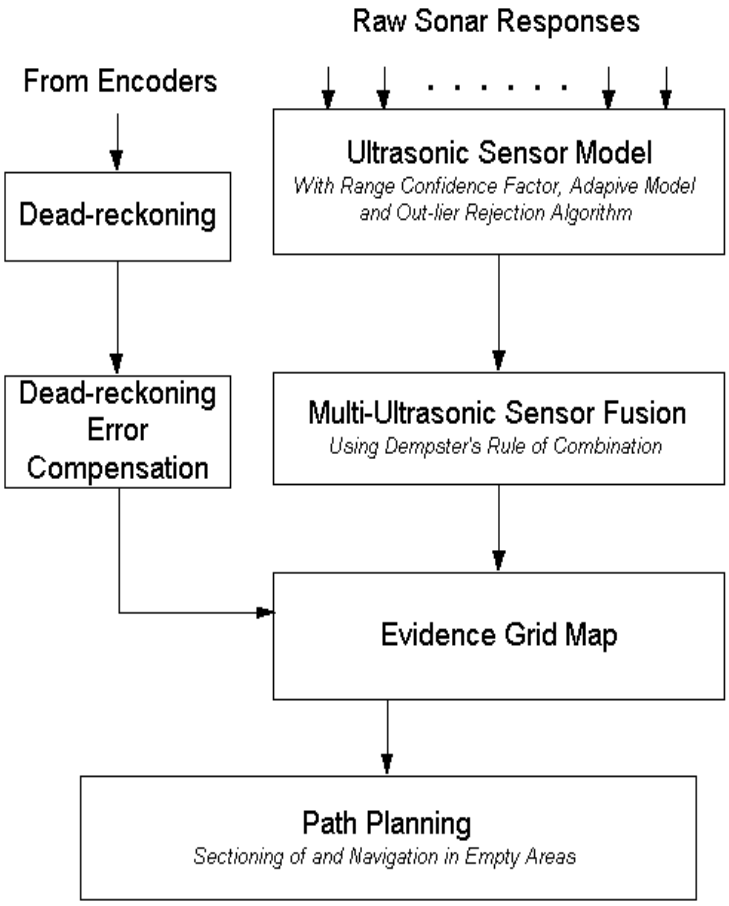

Figure 1.1: The block diagram for multi-ultrasonic sensor fusion and navigation system.

6. To develop path planning algorithm for the autonomous navigation of robot in the area.

1.3 Major Contributions of the Thesis

In an effort to solve problems highlighted earlier, some novel methods have been proposed. In the following, major contributions from this research project are presented.

1. A map of evidence grids has been built for navigation purposes. Brief comparison of the application of Bayesian method [26] and Dempster-Shafer's evidence method [79] in sensor fusion has been made. Dempster's rule of combination has been implemented for multi-ultrasonic sensor fusion on evidence grids.

2. Efforts have been made on reducing the errors in ultrasonic sensor responses caused by specular reflections in confined environments. Detailed analysis of the problem of specular reflections [42] has been made. We have proposed a new method in integrating the conflict factor in evidence theory into an ultrasonic sensor model. This has produced an adaptive model which reduces errors caused by specular reflections. To further eliminate unreliable readings, we have developed a novel algorithm called *outlier rejection algorithm*. The proposed methods have been verified by experimental results.

3. A simple path planning strategy has been developed based on the evidence information in the grid map. The proposed path planning algorithm is easily implemented. It is able to guide the robot through as many empty grid cells as possible.

1.4 Organization of the Thesis

This thesis is organized as the follows:

Chapter 2 presents a brief review of the literature relevant to this project. Available methods proposed by other researchers to solve similar problems are discussed. Issues that remain open are highlighted.

In Chapter 3, we discuss the map building problem. Available methods are discussed. The emphasis here is on the evidence grids which we have adopted as

our sensor fusion framework for map building. Evidence grid based sensor fusion algorithms for map building using the Bayesian and Dempster-Shafer theory are reviewed. A comparison is made between the Dempster-Shafer's evidence theory and Bayesian's probability approach in the multi-ultrasonic sensor fusion. Details in the implementation of the Dempster's rule of combination are covered in this chapter.

In Chapter 4, basic definitions and fundamental characteristics of ultrasonic sensors are given. This is then followed by physical and mathematical descriptions of the ultrasonic sensor model. Special problems associated with ultrasonic sensors like specular reflections are addressed in this chapter.

In Chapter 5, emphasis has been put in reducing unreliable readings arising from specular reflections in ultrasonic sensor responses. The model designed especially for reducing errors caused by specular reflections is given. In this chapter, a novel method which applies the conflict value as an adjusting term is introduced. Furthermore, a new outlier rejection algorithm is given as a complimentary method to deal with outlying errors in ultrasonic responses. Experimental results in practical environments are presented to show the effectiveness of the proposed methods.

In Chapter 6, algorithms for compensating the dead reckoning errors are given with tables of error compensation parameters presented. A simple path planning algorithm has been derived to produce paths in the grid map. The planned paths enable the robot to navigate safely through empty regions in the environment.

Real-time experimental results on a typical confined environments are presented in Chapter 7. Comparisons and discussions on experimental results are given.

In Chapter 8, conclusions are given with recommendation for future work.

Chapter 2

Literature Review

The multi-ultrasonic sensor based mobile robot has been widely discussed by many researchers [3, 59, 43, 34, 35, 41, 42, 10, 12, 17, 28, 82, 25, 48, 88, 91, 5, 56]. Two main issues are normally discussed: map building and autonomous navigation. There are mainly two types of map building methods, gird based and feature based map building methods [51, 72, 49, 24, 92].

The grid based map building was first proposed by Moravec and Elfes [4, 26, 59]. The grid based method divides the workspace into 2 dimensional squares denoted as cells. The states of a cell in the grids can be used to encode a number of properties which are of interest to robot navigation. These include occupancy, reachability, danger, etc [4]. The state of the cell in this thesis has been restricted to represent the occupancy information about the environment since ultrasonic sensors have been used to provide range responses from the surroundings. The state of occupancy can be denoted by probability estimation from sensory information. Sensor responses are projected onto the evidence grids through appropriate sensor models. By integrating the multi-sensory information on the evidence grids, information about

the occupancy in the environment can be obtained [49]. The grid method was first introduced to turn wide angle range measurements into detailed spatial maps [59]. Therefore the grid method is especially effective for using ultrasonic sensors with sparse responses [72]. This approach has been widely used in ultrasonic based robotic applications [53, 19, 16, 41, 9, 1, 51]. The occupancy of environmental areas can be represented using other methods as proposed by Martin Beckerman and E. M. Oblow. They proposed a simple labeling scheme to construct the occupancy map from sonar responses [58]. Approaches to simplify the calculation of the grid method have also been proposed in [37, 38, 56].

The feature based map building methods [24, 49] attempt to model the geometric features of the environment according to the sensor responses [52, 63, 20, 51, 90]. Based on the physical characteristics of ultrasonic sensor and its responses[8, 81], Roman Kuc and Billur Barshan have proposed methods to extract corners and planes from sonar reflections [7, 83]. Kalman filter has also been used in the feature based method for map building and navigation [43]. However, in the case where sensor system is unreliable, for instance those sonar responses corrupted by the specular reflections, the algorithm may be ineffective [49].

A good understanding of ultrasonic methods and applications is necessary for studying the sonar-based robot. Physical principles of ultrasonic sensors can be found in [31, 67, 68, 69]. Sherman Y. T. Lang and etc. have made a thorough testing and modeling of ultrasonic sensor with detailed analysis in ultrasonic responses [84]. The main problems to be faced in using ultrasonic sensors are angular errors in responses, specular reflections and cross-talks in multi-ultrasonic sensors [83, 84, 39, 58, 42, 43, 81, 82, 60, 38, 7]. Michael Drumheller discussed the specular reflection and other sonar response problems in [60]. Johann Borenstein and Yoram Koren

proposed an error eliminating method for cross-talks in [39]. John Hwan Lim and Dong Woo Cho proposed using the *range confidence factor* to reduce the unreliable ultrasonic readings [42].

Early work in sensor fusion can be found in [28, 25]. Linas J. and Waltz E. made a systematic discussion in categorizing methods and problems in multi-sensor fusion [57]. David L. Hall presented mathematical techniques used in multi-sensor fusion [18]. Richard R. Brooks and S. S. Iyengar discussed sensor fusion basics and its development in related topics [74]. Mongi A. Abidi and Ralph C. Gonzalez. presented some application examples for sensor fusion in mobile robots in [61]. Some recent information about the development and potentials in sensor fusion can be found in [6, 62].

Using Kalman filtering in feature-based map building and for sensor fusion has been discussed in details in [30, 43, 66]. Bayesian method was first used for multi-sensory information integration in grid-based methods [26, 3, 4, 19, 41]. Recently, many researchers applied the Dempster-Shafer theory on the evidence grid for multi-sensor fusion [79, 46, 5, 78, 32, 16, 93]. Robin Murphy has used Dempster-Shafer's evidence method in multi-ultrasonic sensor fusion for localization [46]. Andrew Howard and Les Kitchen discussed the use of Dempster-Shafer's evidence method in ultrasonic sensor fusion for speculative environments [5]. In [16], Daniel Pagac. Eduardo, M. Nebot and Hugh Durrant-Whyte discussed the disadvantages of using Bayesian method in grid-based sensor fusion. The Dempster-Shafer's evidence method still has some problems as addressed in [33, 54, 22, 65]. Some researchers proposed new methods based on the Dempster-Shafer's theory. One such example is due to Robin Murphy. She proposed to change the Dempster rule of combination to suit the practical robot situation [80]. Another example is in [32], where Jing-Yu

Yang and Yong-Ge Wu introduced a new energy factor in using Dempster-Shafer's method for multi-sensor fusion.

Localization has always been one of the key issues for autonomous navigation of mobile robots. In [35], errors to be overcome to obtain accurate positional information for localization are analyzed. Localization using ultrasonic sensors are discussed in [82, 43, 11, 91, 92, 48, 49, 50, 24, 9, 47, 10, 1, 27, 14, 55, 51, 20, 56], in which dead reckoning, Kalman filtering and fuzzy logic are all discussed for this purpose. In [11, 50, 24, 10], the grid-based localization methods using ultrasonic sensors are discussed. Kriakopoulos [49, 50] developed Kalman filtering based localization strategy using grid map by feature extraction. The dead reckoning technique has been used widely in the localization [9, 14, 27]. It is simple and easy to be realized. But to make sure that the dead reckoning errors are limited in an acceptable range, compensation has to be done [35, 40, 87] for the dead reckoning.

The path planning strategy should be devised according to the navigation purpose of the robot [88, 75]. Basic requirements for path planning include the optimal path to the destination and the collision free course during navigation [2, 75, 88, 44, 35]. Johann Borenstein and Yoram Koren used vector field histogram on a grid map for fast obstacle avoidance [37]. In [86], path planning using quad-trees was discussed. Alexander Zelinsky presented an exploration algorithm using distance transform for path planning based on the "learning" mode of environment mapping [2]. In this thesis, a simple path planning strategy was used to search free space in the environment based on the grid map produced.

Chapter 3

Sonar-based Map Building

In this chapter, the grid-based map building process and the use of Dempster-Shafer's evidence theory for integrating sensor responses are discussed. Brief review of the mathematical background of the Dempster-Shafer's evidence theory and Baysian theory is presented. Detailed implementation of the multi-ultrasonic sensor fusion using Dempster's rule of combination is also given.

3.1 Map Building

A mobile robot relies on a map for autonomous navigation in an environment. This requires a map building capability. Map building is also a process of constantly updating the representation of knowledge about the robot's surroundings [51]. The task of building accurate environmental maps depends on the on-board sensors. These sensors directly provide the environmental information. We have used ultrasonic sensors for map building as they are easily available, inexpensive and easy to control [72, 56]. Generally, there are two approaches for sonar-based map building

according to the form of data representation [48],

- Feature-based world model

  This approach requires feature-based models for the representation of the environment [50]. Systems of this type construct points, lines or surface descriptions of the environment from sensed data. Kalman filtering and extended Kalman filtering have been used widely in this approach to integrate the sensory information and maintain the map [43]. Neural networks [13] has also been used to extract these geometric features.

- Grid-based world model

  According to [72], grid-based world model is more suitable to the case of using ultrasonic sensors, which suffer from unreliable readings in their responses. This approach allows a statistical expression of confidence in the correctness of data by projecting the sonar response onto the grids [3, 26, 59].

The grid-based world model as the representation for the environment has been used in this project. The evidence grid representation is able to turn wide angle range measurements from ultrasonic sensors into detailed spatial maps. Diffusive multiple sonar readings are able to be integrated on the evidence grids into increasingly confident and detailed map of a robot's surroundings. Successful implementations [3, 26, 5, 37, 46, 19] have proved its effectiveness.

3.2 Evidence Grids

In 1983, Martin C. Martin and Hans P. Moravec of Carnegie Mellon University [59, 26] proposed the evidence grid approach to handle data from inexpensive Polaroid ultrasonic sensors. Ultrasonic sensors are notorious for their wide beams that

leave angular position ambiguous. Unreliable readings caused by specular reflections and misreading due to different irregularities in reflecting surfaces are also common problems. The grid method accumulates occupancy evidence for an array of spatial locations, resolving ambiguities as robot moves. This allows the robot to integrate disparate readings over time, taken from different locations and even with different sensors.

In evidence grids, the world is defined over a discrete spatial lattice in which each grid is actually a discrete state variable [3]. The evidence grids approach is a representation of the world in a probability sense. The evidential information of the surrounding objects is accumulated upon the framework of evidence grids. These information include evidence such as whether a place is empty or occupied by an object. The grid can contain as much information as the system requires, such as occupancy of objects, time, reachability and danger and etc. Many researchers have been very successful in implementing the evidence grids [3, 4, 53, 26, 59, 37, 46, 19, 41, 42, 48, 49, 50, 5]. An example of the evidence grids is shown in Figure 3.1.

Figure 3.1 conveys the idea of the evidence for cells being *unknown* in the sample environment. The actual environment was shown in Figure 3.1a, where there were no objects inside. The Nomad Super Scout II mobile robot [1] was programmed to move to certain positions inside this environment to collect ultrasonic sensor responses. The evidence grids produced by the fusion of the ultrasonic sensory data collected in this environment was shown in Figure 3.1b. For those white cells, they have high evidence for being *unknown*. Cells with gray colors have less evidence accumulated for being *unknown* than white cells. The darker the color in the cell is, the less evidence it has accumulated for being *unknown*. By comparing with the

[1] Please refer to Chapter 7 and Appendix B for more information about Nomad Super Scout II mobile robot

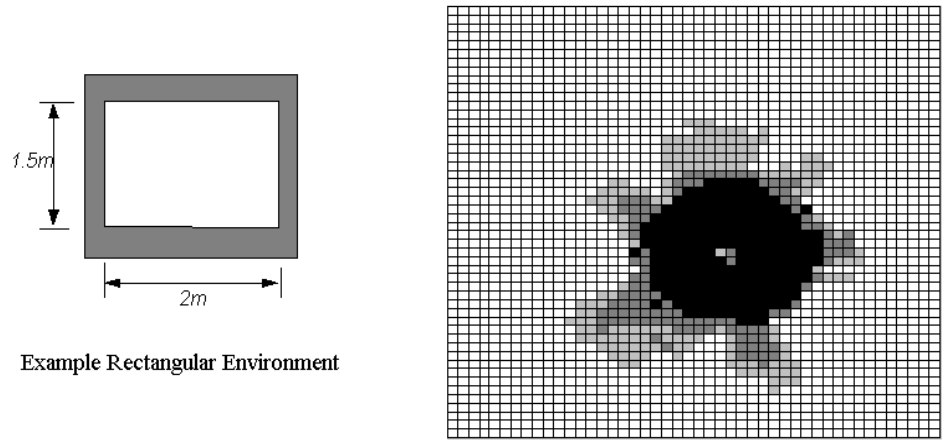

Figure 3.1: Evidence grids example: a. The actual look of a rectangular confined environment. b. The grids produced for evidence of being *unknown* in the sample environment. Sensor responses were collected at the center of the environment by rotating the robot. The grids were initialized as completely *unknown* at the start with all cells in white. The whiter the cell is, the more evidence for being *unknown* there is for the cell.

actual view of the confined space given in Figure 3.1a, the dark areas in Figure 3.1b have actually been sensed by sonars. White areas like those beyond boundaries are not viewable to the sensor so they have high evidence for being *unknown*. However, several cells at the center in Figure 3.1b also have relatively high evidence for being *unknown*, this is because that sensors failed to see that part correctly. This was most probably due to problems like specular reflections.

With the appropriate sensor model to convert raw sensor responses to the evidence, multi-sensory information can be fused to produce the grid map of the surroundings. Basically, two methods have been used to complete the sensor fusion on the evidence grids, Bayesian method and Dempster-Shafer's evidence method [3, 59, 26, 42]. In the next section, brief reviews of the two methods are given first with comparisons between the two methods in the application of multi-sensor fusion.

3.3 Bayesian Method and Dempster-Shafer's Method

3.3.1 Brief Review of Bayesian Method

Bayesian method was widely used for the multi-sensory information integration on evidence grids. The theoretical details can be found in [21, 85] and the implementation information in [3, 19]. In the following, a review of the Bayesian theory is briefly presented.

Let $P(A|B)$ be the *conditional probability* for event A given the information from event B, where for the two events A and B, $P(A) > 0$ and $P(B) > 0$, then,

$$P(A|B) = \frac{P(A \cap B)}{P(B)} \tag{3.1}$$

where $P(A \cap B)$ is the probability for the *intersection* set of A and B, with

$$A \cap B = \{x | x \in A \text{ and } x \in B\} \tag{3.2}$$

Other useful forms of Equation 3.1 can be obtained as,

$$P(A \cap B) = P(A|B)P(B) \tag{3.3}$$

$$= P(B|A)P(A) \tag{3.4}$$

Let $\{B_i\}$ be a countable set of exhaustive events and $P(B_i) > 0$. Let A be an arbitrary event, then the *total probability rule* says,

$$P(A) = \sum_{i \in I} P(B_i)P(A|B_i) \tag{3.5}$$

In Equation (3.5),

1. $P(B_i) > 0$ *and* $B_i \cap B_j = \phi \qquad (i \neq j, i, j \in I)$
2. $A = \bigcup_{i \in I}(A \cap B_i)$

where $I \subseteq \{1, 2, ..., n\}$. Based on the *conditional probability* and *total probability rule* given in Equations (3.1) to (3.5), the Bayesian formula can be generalized as [21],

$$P(B_j|A) = \frac{P(A|B_j) \cdot P(B_j)}{\sum_{i \in I} P(B_i)P(A|B_i)} \tag{3.6}$$

where $\{B_i\}$ is a countable set of exhaustive events such that $P(B_i) > 0$ and A is an event with $P(A) > 0$.

In the evidence grids method, the knowledge of the world based on the sensory information perceived can be expressed as a conditional probability. In Equation (3.6), the event B_i represents the state of a cell i in the grids [26, 3, 59]. In order to tell the robot how the outside world looks like from the occupancy information, the state of each cell has been defined as either *occupied* or *empty*. Therefore, B_i=$\{$*occupied*$\}$ or $\{$*empty*$\}$. If event A is the event representing a given sensor reading, then $P(B_i|A)$ represents the probability of a cell state being *occupied* or *empty* given this sensor reading. $P(\{occupied\})$+$P(\{empty\})$=1 since the two events, $\{$*occupied*$\}$ and $\{$*empty*$\}$, are exclusive and exhaustive. Using Bayesian method, we can have the following implementation equations as [3, 26, 19],

$$P(S_i^{occ}|M = R) = \frac{P(M = R|S_i^{occ}) \cdot P(S_i^{occ})}{P(M = R|S_i^{occ}) \cdot P(S_i^{occ}) + P(M = R|S_i^{emp}) \cdot P(S_i^{emp})} \tag{3.7}$$

$$P(S_i^{emp}|M=R) = \frac{P(M=R|S_i^{emp}) \cdot P(S_i^{emp})}{P(M=R|S_i^{occ}) \cdot P(S_i^{occ}) + P(M=R|S_i^{emp}) \cdot P(S_i^{emp})} \quad (3.8)$$

where, $P(S_i^{occ}|M=R)$ means the probability that the state of cell i is *occupied* given the sensor measurement M is R. It goes the same for $P(S_i^{emp}|M=R)$. $P(S_i^{emp})$ and $P(S_i^{occ})$ are existing old evidence of cell i. $P(M=R|S_i^{emp})$ and $P(M=R|S_i^{occ})$ are evidence obtained through the sensor model. So the cell state can be updated by Equation (3.7) and (3.8) whenever there is a new sensor information $M=R$. As Equation (3.7) and (3.8) are commutative and associative [53, 26], multi-sensory information can be incorporated using sequential updating equations. The sequential updating equations in Bayesian method can be found in in Appendix A.

3.3.2 Dempster-Shafer's Evidence Method

Another frequently used approach for sensor fusion on evidence grids, the Dempster-Shafer's evidence method, is briefly reviewed in this section. Before presenting the formulas for sensor fusion, basic definitions of some functions in Dempster-Shafer's evidence theory are given. More mathematical details can be found in [23, 33].

Let θ be a finite non-empty set, called the *frame of discernment*, or *FOD*. θ is a set of propositions about the exclusive and exhaustive possibilities in a domain. In evidence grids where each cell is either *empty* or *occupied*, the *frame of discernment* θ is then defined as,

$$\theta = \{occupided, empty\} \quad (3.9)$$

The *power set* of θ, denoted as 2^θ, is the collection of all subsets of θ. When θ is

as given in Equation (3.9), 2^θ is,

$$2^\theta = \{\phi, \{occupided\}, \{empty\}, \{occupided, empty\}\} \tag{3.10}$$

where ϕ is the *empty set.* The number of elements in the set θ is called the cardinality of θ, denoted as $|\theta|$.

In Dempster-Shafer's evidence theory, a portion of the belief can be committed to a proposition while the remainder need not be committed to its negation. While in Bayesian theory, whenever one commits only a portion of one's belief to a proposition, one must commit the remainder to its negation. Therefore, in Dempster-Shafer's evidence theory, it is possible to partition all of one's belief among the different subsets of the whole set θ, assigning to each subset A that portion that is committed to A and to nothing smaller. Therefore the *mass function* is given in the following for this purpose.

A function m,

$$m : 2^\theta \longrightarrow [0, 1]$$

is called a *mass function* [23] if it satisfies,

1. $m(\phi) = 0$
2. $\sum_{X \subseteq \theta} m(X) = 1$

The mass function is a *basic probability assignment to all subsets X of* θ. $m(A), A \subseteq 2^\theta$ is called *A's mass or basic probability value.* It represents the exact amount of belief committed to the proposition represented by the subset A of θ. Any subset A that satisfies $m(A) > 0$ is called a *focal element* of the mass function m over θ. Since the quantity $m(A)$ measures the belief committed exactly to A, $A \subset \theta$, to obtain the measure of the total belief committed to A, those quantities representing

beliefs from all the proper subset of A must also be included. Therefore a portion of belief committed to one proposition is thereby committed to any other proposition it implies, which means a portion of belief committed to one subset is also committed to any subset containing it. So $belief function$ is defined for this purpose as following.

A function

$$bel : 2^{\theta} \longrightarrow [0, 1]$$

is called a *belief function* [23] if it satisfies,

1. $bel(\phi) = 0$
2. $bel(\theta) = 1$
3. for any collection $A_1, A_2, \ldots, A_n, (n \geq 1)$ of subsets of θ

$$bel(\bigcup_{i=1}^{n} A_i) \geq \sum_{I \subseteq \{1,2,\ldots,n\}, I \neq \phi} (-1)^{|I|+1} bel(\bigcap_{i \in I} A_i)$$

The inversion between the mass function and the belief function [23] is given as,

$$bel(A) = \sum_{X \subseteq A} m(X) \tag{3.11}$$

$$\leftrightarrow.$$

$$m(A) = \sum_{X \subseteq A} (-1)^{|A-X|} bel(A) \tag{3.12}$$

for all $A \subseteq \theta$.

The Dempster-Shafer's evidence theory is capable of treating both the *ignorance* and *uncertainty*. The ignorance is represented by $1 - bel(A)$, if $A, A \subset \theta$, represents

the proposition of interest. For uncertainty of the same proposition represented by A, it is represented by the belief one has for the negation, i.e. $bel(\bar{A})$.

$$\begin{aligned} 1 - bel(\bar{A}) &= \sum_{X \subseteq \theta} m(X) - \sum_{X \subseteq \bar{A}} m(X) \\ &= \sum_{X \not\subseteq \bar{A}} m(X) \\ &= \sum_{X \cap A \neq \phi} m(X) \\ &\geq \sum_{X \subset A} m(X) \end{aligned}$$

Therefore, we have

$$bel(A) + bel(\bar{A}) \quad \square \quad 1 \tag{3.13}$$

Thus there exists a *belief interval* between $bel(A)$ and $1 - bel(\bar{A})$,

$$belief\ interval \quad = \quad [bel(A)\ ,\ 1 - bel(\bar{A})] \tag{3.14}$$

However in the case of Bayesian method, it won't be able to differentiate the ignorance and uncertainty. In Equation (3.13), when $1 - bel(\bar{A}) = bel(A)$, so $bel(A) + bel(\bar{A}) = 1$, Dempster Shafer's method reduces to the Bayesian method since $A \cap \bar{A} = \phi$. In Bayesian case, probabilities are assigned to singletons as shown Equation (3.6), $B_i \cap B_j = \phi$, $i \neq j$. In the case of application on evidence grids, $P(\{occupied\}) = 1 - P(\{empty\})$. For a set A called a *singleton*, it satisfies,

$$A \quad = \quad \{x\} \qquad x \in \theta, \qquad A \subset 2^{\theta} \tag{3.15}$$

In our case, Bayesian only assigns non-zero probabilities to singletons of θ to

satisfy $P(\{occupied\})+P(\{empty\}) = 1$. We must divide out basic probability assignment among singleton propositions [33]. Therefore, we have to know enough to assign mass to every singleton element. But sometimes this will be very difficult [5, 46]. For example, for each cell in the evidence grids, $P(\{occupied\})$ is available from the sensor data. To satisfy $P(\{occupied\})+P(\{empty\}) = 1$, $P(\{empty\})$ is assigned as 1-$P(\{occupied\})$. However, in the case that no evidence for *empty* is available, $P(\{empty\})$ should actually be zero. Hence, Bayesian lacks the ability of treating the *ignorance* that Dempster-Shafer's evidence theory has. Considering these advantages over Bayesian method, we have preferred Dempster-Shafer's evidence method in realizing our multi-sensor fusion algorithm.

3.3.3 Dempster's Rule of Combination

Using the Dempster's rule of combination [23, 33], multiple sensory readings can be fused successfully. Let m_1 and m_2 be mass functions on the same frame of discernment θ, the combination of two mass functions is then given as,

$$m(A) = \frac{1}{1-\square} \sum_{X\cap Y=A, A\neq\phi} m_1(X)m_2(Y) \tag{3.16}$$

where $A \neq \phi, A \subset \theta$ and the term $\square$ is defined as,

$$\square = \sum_{X\cap Y=\phi} m_1(X)m_2(Y) \tag{3.17}$$

which measures the extent of conflict between the two mass functions $m_1(X)$ and $m_2(Y)$. $\square$ acts to normalize the other sum terms in order to meet the conditions in mass function definition. The mass function given by Equation (3.16) is also called

the *orthogonal sum* of m_1 and m_2 and denoted as,

$$(m_1 \oplus m_2)(A) \;=\; \frac{1}{1-\square} \sum_{X \cap Y = A} m_1(X) m_2(Y) \tag{3.18}$$

The following is a simple example to show how the Dempster's rule of combination is actually used.

Example 3.1 *Suppose* θ*=*$\{a,b,c\}$ *and* $m_1(\{a,b\})$*=0.5,* $m_1(\theta)$*=0.5,* m_1*(elsewhere)=0;* $m_2(\{b,c\})$*=0.4,* $m_1(\theta)$*=0.6,* m_1*(elsewhere)=0; Calculate* $m_1 \oplus m_2$*.*

Solution First, the power set of θ is,

$$2^\theta = \{\phi, \{a\}, \{b\}, \{c\}, \{a,b\}, \{b,c\}, \{a,c\}, \{a,b,c\}\}$$

$\square$ is calculated as,

$\square = \sum_{X \cap Y = \phi} m_1(X) m_2(Y)$

$= m_1(\{a\})m_2(\{b,c\}) + m_1(\{b\})m_2(\{a,c\}) + m_1(\{c\})m_2(\{a,b\})$

$\quad + \; m_1(\{a,c\})m_2(\{b\}) + m_1(\{a,b\})m_2(\{c\}) + m_1(\{b,c\})m_2(\{a\})$

$\quad + \; m_1(\phi)m_2(\{a,b,c\}) + m_1(\phi)m_2(\{a,b,c\})$

$= 0$

therefore,

$(m_1 \oplus m_2)(\{a\}) = \frac{1}{1-\square}[m_1(\{a\})m_2(\{a,c\}) + m_1(\{a\})m_2(\{a,b\})$

$\quad + \; m_1(\{a,b\})m_2(\{a\}) + m_1(\{a,c\})m_2(\{a\}) + m_1(\{a\})m_2(\{a,b,c\})$

$\quad + \; m_1(\{a,b,c\})m_2(\{a\}) + m_1(\{a,c\})m_2(\{a,b\}) + m_1(\{a,b\})m_2(\{a,c\})]$

$= 1 \times (0 + 0 + 0 \times 0.6 + 0.5 \times 0 + 0 + 0.5 \times 0 + 0 + 0.5 \times 0)$

$= 0$

$(m_1 \oplus m_2)(\{b\}) = \frac{1}{1-\square}[m_1(\{b\})m_2(\{b,c\}) + m_1(\{b\})m_2(\{a,b\})$

$\quad + \; m_1(\{a,b\})m_2(\{b\}) + m_1(\{b,c\})m_2(\{b\}) + m_1(\{b\})m_2(\{a,b,c\})$

$\quad + \; m_1(\{a,b,c\})m_2(\{b\}) + m_1(\{a,b\})m_2(\{b,c\}) + m_1(\{b,c\})m_2(\{a,b\})]$

$= 1 \times (0 \times 0.4 + 0 + 0 \times 0.6 + 0.5 \times 0 + 0 + 0.5 \times 0 + 0.5 \times 0.4 + 0)$

$$= 0.2$$

$$(m_1 \oplus m_2)(\{c\}) = \frac{1}{1-\square}[m_1(\{c\})m_2(\{a,c\}) + m_1(\{c\})m_2(\{b,c\})$$
$$+ \ m_1(\{a,c\})m_2(\{c\}) + m_1(\{b,c\})m_2(\{c\}) + m_1(\{c\})m_2(\{a,b,c\})$$
$$+ \ m_1(\{a,b,c\})m_2(\{c\}) + m_1(\{a,c\})m_2(\{b,c\}) + m_1(\{b,c\})m_2(\{a,c\})]$$
$$= 1 \times (0 + 0 \times 0.4 + 0 \times 0.6 + 0 + 0 + 0.5 \times 0 + 0 \times 0.4 + 0)$$
$$= 0$$

$$(m_1 \oplus m_2)(\{a,b\}) = \frac{1}{1-\square}[m_1(\{a,b\})m_2(\{a,b\}) + m_1(\{a,b\})m_2(\{a,b,c\})$$
$$+ \ m_1(\{a,b,c\})m_2(\{a,b\})]$$
$$= 1 \times (0.5 \times 0 + 0.5 \times 0.6 + 0.5 \times 0)$$
$$= 0.3$$

$$(m_1 \oplus m_2)(\{a,c\}) = \frac{1}{1-\square}[m_1(\{a,c\})m_2(\{a,c\}) + m_1(\{a,c\})m_2(\{a,b,c\})$$
$$+ \ m_1(\{a,b,c\})m_2(\{a,c\})]$$
$$= 1 \times (0 + 0 \times 0.6 + 0.5 \times 0)$$
$$= 0$$

$$(m_1 \oplus m_2)(\{b,c\}) = \frac{1}{1-\square}[m_1(\{b,c\})m_2(\{b,c\}) + m_1(\{b,c\})m_2(\{a,b,c\})$$
$$+ \ m_1(\{a,b,c\})m_2(\{b,c\})]$$
$$= 1 \times (0 \times 0.4 + 0 \times 0.6 + 0.5 \times 0.4)$$
$$= 0.2$$

$$(m_1 \oplus m_2)(\{a,b,c\}) = \frac{1}{1-\square}[m_1(\{a,b,c\})m_2(\{a,b,c\})]$$
$$= 1 \times (0.5 \times 0.6)$$
$$= 0.3$$

The combinations of n mass functions is given in Equation (3.19) [23]. Let

$m_1, m_2, \ldots, m_n$ be mass functions over the same frame of discernment θ, then,

$$(\bigoplus_{q=1}^{n} m_q)(A) = \frac{1}{1-\square_n} \sum_{\bigcap_{j=1}^{n} X_j = A} (\prod_{j=1}^{n} m_j(X_j)) \tag{3.19}$$

where $\square_n$, which represents the conflict among the n mass functions, is defined as,

$$\square_n = \sum_{\bigcap_{i=1}^{n} X_i = \phi} (\prod_{j=1}^{n} m_j(X_j)) \tag{3.20}$$

Note if $\square$ or $\square_n = 1$, the denominator of the normalization term would be zero, then the mass function would approach infinity. This means the *total contradiction* of the mass functions [23, 33].

3.4 Implementation

The Dempster-Shafer evidence method was implemented on the evidence grids representing the environment. Each grids cell is either *empty* or *occupied* on evidence grids. Practically, a sensor is a source of evidence about a set of propositions, the *focal elements.* Hence the *frame of discernment, FOD* is the set of propositions with evidence from sensory information. As given in Equation (3.9) and Equation (3.10), the *frame of discernment, FOD* is defined as,

$$\theta = \{occupied,\ empty\} \tag{3.21}$$

and 2^θ is given as,

$$2^\theta = \{\phi, \{occupied\},\ \{empty\},\ \{empty,\ occupied\}\} \tag{3.22}$$

With no *a priori* knowledge, the evidence of a cell i in the evidence grids has been initialized as,

$$m^i(\{occ\}) = m^i(\{occupied\}) = 0 \tag{3.23}$$

$$m^i(\{emp\}) = m^i(\{empty\}) = 0 \tag{3.24}$$

$$m^i(\{unk\}) = m^i(\{unknown\} = \{empty,\ occupied\}) = 1 \tag{3.25}$$

This means no evidence for either *occupied* or *empty* in an unknown environment. Raw sensor responses to evidential values through appropriate sensor models. The use of ultrasonic sensor model is introduced in Chapter 4. Therefore, sensory information can be expressed by corresponding evidential functions. After evidence from sensory information have been successfully extracted from raw sensor responses, the combination rule can be applied to update the new evidence. If we use the subscript "o" for the old existing evidence, "s" for the evidence from the sensor, "n" for the new evidence from the fusion, the sensor fusion implementation is expressed in the following Equation (3.26)

$$m_n^i(\{A\}) = (m_o^i \otimes m_s)(\{A\}) \quad A \in 2^\theta \ and \ i = 1, ..., N \tag{3.26}$$

Where N is the maximum number of cells in the evidence grids. Equation (3.27) to (3.29) below were used to implement the multi-ultrasonic sensor fusion for cell i on the evidence grids.

$$m_n^i(\{occ\}) = \frac{m_o^i(\{occ\})m_s(\{occ\}) + m_o^i(\{occ\})m_s(\{unk\}) + m_o^i(\{unk\})m_s(\{occ\})}{1 - m_o^i(\{occ\})m_s(\{emp\}) - m_o^i(\{emp\})m_s(\{occ\})} \tag{3.27}$$

$$m_n^i(\{emp\}) = \frac{m_o^i(\{emp\})m_s(\{emp\}) + m_o^i(\{emp\})m_s(\{unk\}) + m_o^i(\{unk\})m_s(\{emp\})}{1 - m_o^i(\{occ\})m_s(\{emp\}) - m_o^i(\{emp\})m_s(\{occ\})} \tag{3.28}$$

$$m_n^i(\{unk\}) = \frac{m_o^i(\{unk\})m_s(\{unk\})}{1 - m_o^i(\{occ\})m_s(\{emp\}) - m_o^i(\{emp\})m_s(\{occ\})} \tag{3.29}$$

where $m_o^i(A), A \in 2^\theta$ is the existing evidence for cell i . $m_n^i(A), A \subseteq 2^\theta$ is evidence of cell i to be updated. $m_s(A), A \subseteq 2^\theta$ is the evidence from the sensor data. □ in this case is then given in Equation (3.30) as,

$$\square = m_o^i(\{occ\})m_s(\{emp\}) + m_o^i(\{emp\})m_s(\{occ\}) \tag{3.30}$$

Figure 3.2 shows the flow chart of the multi-ultrasonic sensor fusion. According to the flow chart given in Figure 3.2, there are 3 loops in the sensor fusion algorithm. Therefore the order of complexity of the sensor fusion algorithms is $O(n^3)$.

The following example shows how the cell state is updated in the process shown in Figure 3.2 through Equations (3.27) to (3.29).

Example 3.2 *Given $m_s(\{emp\})$ = 0.4, $m_s(\{occ\})$ = 0.2, $m_s(\{unk\})$=0.4; update the m_o^i for m_n^i with $m_o^i(\{occ\})$=0.8, $m_o^i(\{emp\})$=0.1, $m_o^i(\{unk\})$=0.1.*

Solution

$$m_n^i(\{occ\}) = \frac{0.8\times0.2+0.8\times0.4+0.1\times0.2}{1-0.8\times0.4-0.1\times0.2} = \frac{0.50}{0.66} \approx 0.7576$$

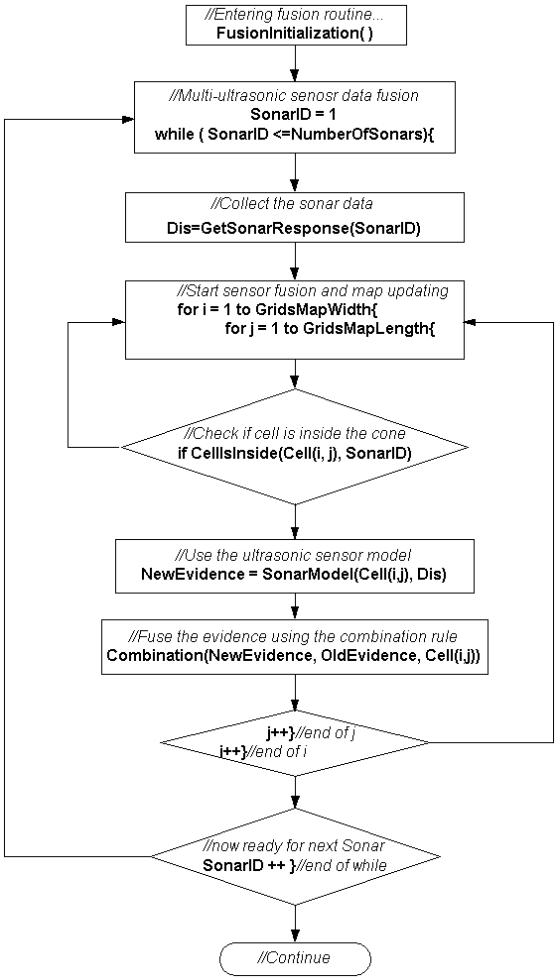

Figure 3.2: Flow diagram for the multi-ultrasonic sensor fusion process.

$$m_n^i(\{emp\}) = \frac{0.1\times0.4+0.1\times0.4+0.1\times0.4}{1-0.8\times0.4-0.1\times0.2} = \frac{0.12}{0.66} \approx 0.1818$$
$$m_n^i(\{occ\}) = \frac{0.1\times0.4}{1-0.8\times0.4-0.1\times0.2} = \frac{0.04}{0.66} \approx 0.0606$$

To obtain $m_s(A)$, we need a sensor model to convert the raw ultrasonic response into evidence values. Since the evidence is updated by the new sensory information from ultrasonic sensors, it is extremely important to extract sensory information accurately from raw ultrasonic responses. This job is done by the ultrasonic sensor model that is to be discussed in the next chapter.

Chapter 4

Using Ultrasonic Sensors

Sensor model is the mathematical description of the sensory data obtained from the physical sensing units. Ultrasonic sensor model is used to project the raw range information onto the evidence grid. In our work, special attention have been paid in dealing with the specular reflection problem in sonar responses. In this chapter, we first introduce characteristics of the ultrasonic sensor. A sonar model, which is able to reduce unreliable sonar readings and is adaptive to the environment, is given, together with some experimental results.

4.1 Why Use Ultrasonic Sensors?

Ultrasonic sensors are used in this project to build a map of the environment. The map contains information of the boundaries of the environment and obstacles inside which are to be used in the navigation. The ultrasonic sensor provides range

information based on the *time of flight(TOF)* principle as given in Equation (4.1),

$$d = vt \tag{4.1}$$

where d is the *round-trip distance*, v is the *speed of propagation* of the pulse and t is the *elapsed time*. According to [43, 72], ultrasonic TOF ranging system is today the most commonly used technique employed on indoor mobile robotics systems, primarily due to the following reasons,

1. Low cost

   Cost is a very important element in developing service robots for everyday use. Ultrasonic sensors are widely available at very low prices. In this aspect, the ultrasonic sensor has great advantage over the laser scanner and other sensors such as the camera [70, 71].

2. Easy maintenance

   For practical use, maintenance is an important issue. Ultrasonic sensors are compact in design, light in weight and very reliable. It is also easy to interface these sensors with other sub-systems of the robot [67, 68, 69] because the output and input to this module are standard TTL signals. For example, the ultrasonic sensor module can be directly connected to I/O ports of the microcontroller or PC, which work as the navigation or control subsystem in a robot system.

3. High range detection accuracy

   The range detection from the ultrasonic sensor is very accurate. For Polaroid 600 series, a typical accuracy is 1% of the reading over the entire range [67, 69, 70, 71]. Ultrasonic sensor is able to provide range information from 0.1524m

(6 inches) to 10.668m (35 feet).

4.2 Physical Descriptions of Ultrasonic Sensors

The only distinction between audible sound and ultrasound is that the latter cannot be heard by the human ears [31, 7]. The theory of ultrasonic propagation is thus exactly the same as that of audible sound. So with the speed denoted as c, ultrasound must satisfy the basic Equation (4.2)

$$c = \frac{\lambda}{T} = \lambda f \tag{4.2}$$

where λ is the ultrasound wave length, T is the period, f is the frequency. The ultrasound wave also satisfies all the reflection, diffraction and attenuation principles of normal audible sound. Since we are using the sonar to provide the range information, the speed of sound is our main concern. The speed c varies in different propagation media and at different temperatures. For ultrasound traveling in air, the relationship between the speed c and the ambient temperature T satisfies the following expression,

$$c = 331.4\sqrt{\frac{T}{273}} \qquad m/sec \tag{4.3}$$

Here the T is in degrees Kelvin. An approximate relationship valid over a temperature range from -30 degrees Celsius to +30 degrees Celsius is given by,

$$c = 331.4 + 0.607T_c \;\; m/sec \tag{4.4}$$

where T_c is the ambient temperature in degrees centigrade. For accurate measurement, a correction for changes in the ambient temperature must be made. For our purposes, we shall use $c = 346$ m/s for air-conditioned laboratory environment, corresponding to an ambient temperature of about 24 degrees centigrade.

The Polaroid ultrasonic transducer employed in this project is the 600 series . This electrostatic transducer comes with the accompanying 6500 series sonar ranging module. Figure 4.1 gives the sound intensity pattern of the Polaroid ranging module while Figure 4.2 gives an more intuitive pattern [67]. This ranging module is

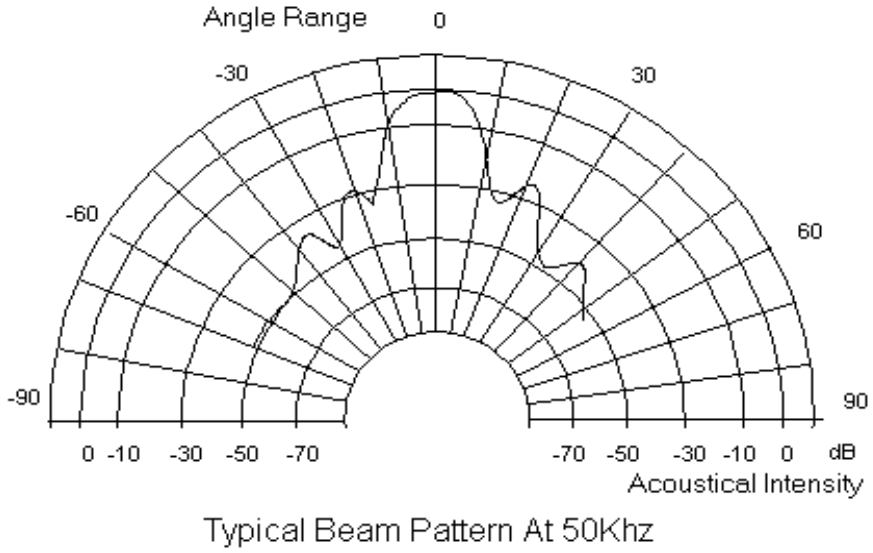

Figure 4.1: Typical beam pattern of Polaroid ultrasonic sensor.

able to measure distance from 0.1524 m (6 inches) to 10.668 m (35 feet) with a typical accuracy of $\pm 1\%$ over the entire range. The module contains two important components. One is the transducer which also acts as a receiver. The other is the driving circuit board based on two TTL ICs, TL851 as the sonar ranging controller and TL852 sonar echo receiver [69]. When the energy of the ultrasound traveling back from the reflected object is high enough to trigger the thresholding circuit, the ranging unit reports a response.

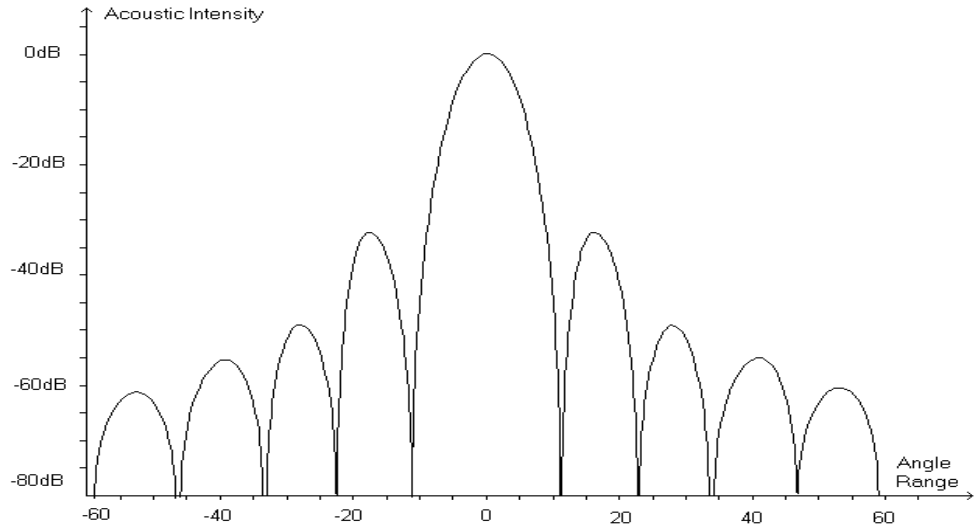

Figure 4.2: Radiated sound intensity pattern for Polaroid transducer. The x axis is the azimuth with respect to the transducer axis, in degrees, and the y axis shows acoustic intensity in dB.

It is generally accepted that the range of a sonar response forms a sector with an opening angle of about 30 degrees [43], as shown in Figure 4.3. The R is the range response produced from the sonar ranging system and $\alpha = 15^o$ is the half opening angle of the sonar cone. The existence of the sonar cone causes the angular ambiguity in sonar responses.

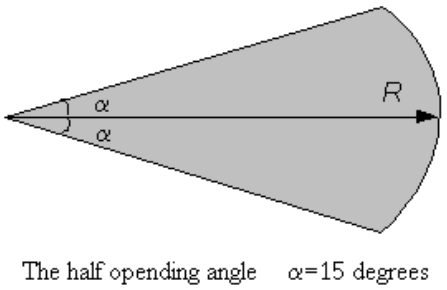

Figure 4.3: The shaded area is the sonar cone with a spanning angle of 30^o.

To have a better understanding of ultrasonic sensors, we show sonar responses from two typical geometrical shapes, a wall and a corner. According to Figure 4.4, the central feature of the response is an arc of circle, centered with respect to the

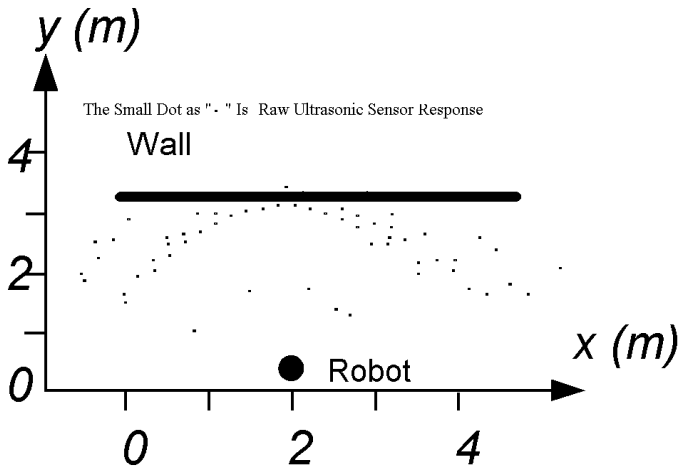

Figure 4.4: Typical sonar responses from a wall. Data collected by firing the sonar ring of 16 ultrasonic sensors on Nomad Super Scout robot. The robot was rotated at the same position.

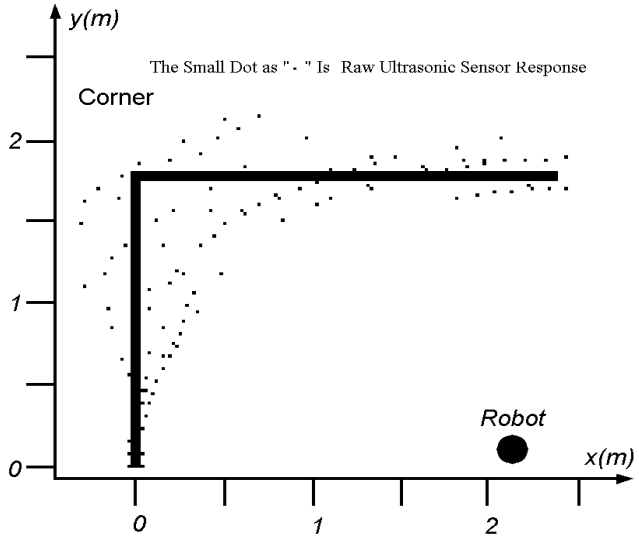

Figure 4.5: Typical sonar responses to a corner. Data collected by firing the sonar ring of 16 ultrasonic sensors on Nomad Super Scout robot. The robot was rotated at the same position.

normal of the wall surface. This pattern is caused by the main lobe whose energy is very high and the thresholding circuit is promptly triggered. When the normal to the surface leaves the main lobe, the energy is reflected away from the source.

Similar case happens to the secondary lobe: if the normal to the surface is within the secondary lobe, the sound gets reflected. As the secondary lobe has lower energy than the main one, there is a range error because the thresholding circuit takes more time to be triggered. For the case shown in Figure 4.5, the central pattern is an arc of circle centered about the corner. It comes from a double specular reflection at the corner. The neighboring arcs can be attributed to the secondary lobes. The left-most and right-most arcs come from specular reflections on the corner's sides. We have to note that when the sonar is close to the corner, it is difficult to predict where the returned echo is actually coming from. The multi-sonar responses in Figure 4.5 appear seriously noisy. There are some responses that show range values far beyond the physical boundaries of the wall and the corner. The noisy patterns of sonar responses are due to physical characteristics of Polaroid ultrasonic sensor, and also due to the interaction between sensors and the operating environment. Details are discussed in the next section.

4.3 Problems in Sonar Responses

Ultrasonic sensors suffer from unreliable sonar responses [63, 81, 43] from the environment. For sonar-based mobile robot in confined space, special attention should be paid to these problems. By confined space, we mean a space whose width and depth are no more than 6 meters. The space is normally a closed environment. The typical example of this space is a toilet or a kitchen. As our concern is the navigation of robot in confined spaces using multi-sonars, we must understand why there are such unreliable readings in ultrasonic sensor responses. Two major problems are discussed in the following.

4.3.1 Angular Uncertainty

The angular uncertainty means the uncertainty in the angle information of a sonar response from a detected object. Figure 4.6 conveys the idea. When an ultrasonic

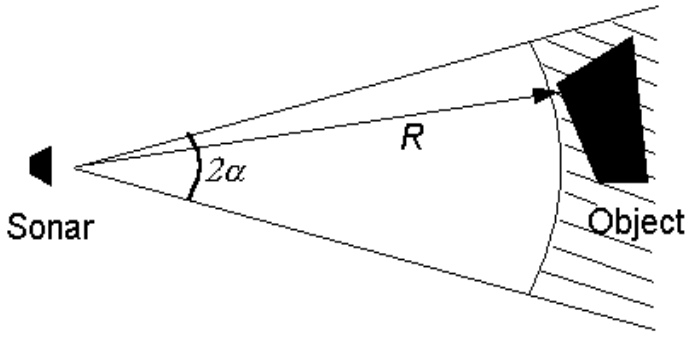

Figure 4.6: Angular error of an ultrasonic sensor. α is the half opening angle of sonar cone, R is a sonar response

sensor gets a range response of R meters, the response simply represents a cone within which the object may be present. There is no way to pin-point exactly where the position of the object is. As shown in Figure 4.6, the opening angle of the ultrasonic sensor is 2α, the object can be anywhere in the shaded region for the response R. For practical purpose, we are only interested in total beam width of about 30 degrees as the boundary of the sonar cone [67].

4.3.2 Specular Reflection

Specular reflection [60, 42] refers to the sonar response that is not reflected back directly from the target object. In specular reflection, the ultrasound is reflected away from the reflecting surface, which results in longer range reporting or missing the detection of object all together.

The specular reflection is due to different relative positions of the ultrasonic transceiver and the reflecting surfaces. Figure 4.7 shows sonar responses in two

different situations. In Figure 4.7a, the sonar transceiver axis is perpendicular to the reflection surface, so most of the sound energy is reflected directly back to the ultrasonic sensor and only a very small percentage of the energy is scattered in other directions. However in Figure 4.7b, because the sonar transceiver is not perpendicular to the surface, much energy will be reflected away. This produces a longer range reporting or even no response at all. The amount of reflected sound

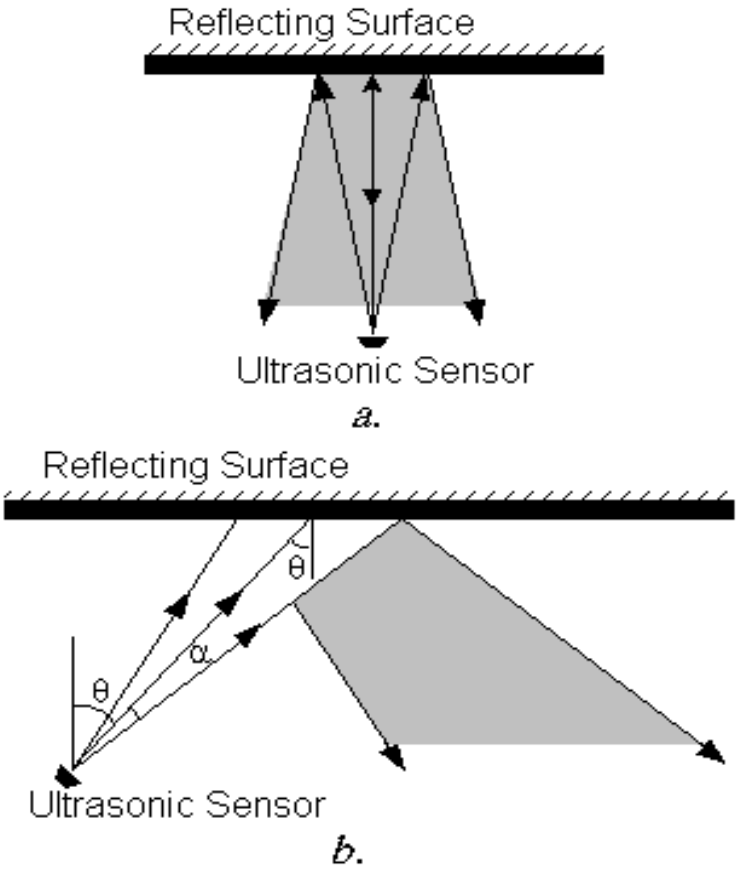

Figure 4.7: Specular reflections

energy depends strongly on the surface structure of the obstacle and the incidence angle [81]. To obtain a highly diffusive reflection from an obstacle, the size of the irregularities on the reflecting surface should be comparable to the wavelength of the incident sound waves [36]. This effect is observed frequently. The pulse emitted

from the Polaroid device has a frequency of about 55kHz and a wave length of about a quarter of an inch [67, 68]. This means unless the sensed surface has irregularities whose sizes are of the same order of the sound wavelength, the beam will be reflected instead of being scattered. In this case there may either be no echo or an echo produced after reflection off some object other than the target. These false reflections occur whenever the incidence angle of the beam θ is greater than a critical angle. The critical incidence angle may range from 7 or 8 degrees (for glass) to nearly 90 degrees for rough surface. For ultrasonic sensor, the critical incidence angle for a reliable detection of a "smooth" surface has been said to be about 25 degrees [82, 58]. The surface of most objects in the real world can be considered as specular according to the Equation (4.5) and Equation (4.6) [42],

$$\Delta\Omega = \frac{4\pi H}{\lambda} sin\beta \tag{4.5}$$

$$\beta = \frac{\pi}{2} - \theta \tag{4.6}$$

where, $\Delta\Omega$ is the phase difference, λ is the wave length, θ is the incidence angle, H is the height of surface irregularities. In the above equations, when the phase difference $\Delta\Omega$ holds, $sin(\beta)$ will decrease, when the incidence angle θ increases. As $\frac{4\pi}{\lambda}$ remains as constant, H will also increase. In this case, as shown in Figure 4.7a, if the incident angle θ of the sound wave on an object with a specular surface is greater than half the aperture of the sensor beam, α, the sensor would fail to detect the echo signal [42, 60, 36].

4.4 Ultrasonic Sensor Model

To integrate multiple sensory readings on the evidence grid, we must use a sensor model to convert the range information into evidence values. The ultrasonic sensor model introduced in [26, 3, 46] is given in this section. The profile of this model is give in Figure 4.8. When there is a range response as R, for a cell in the evidence

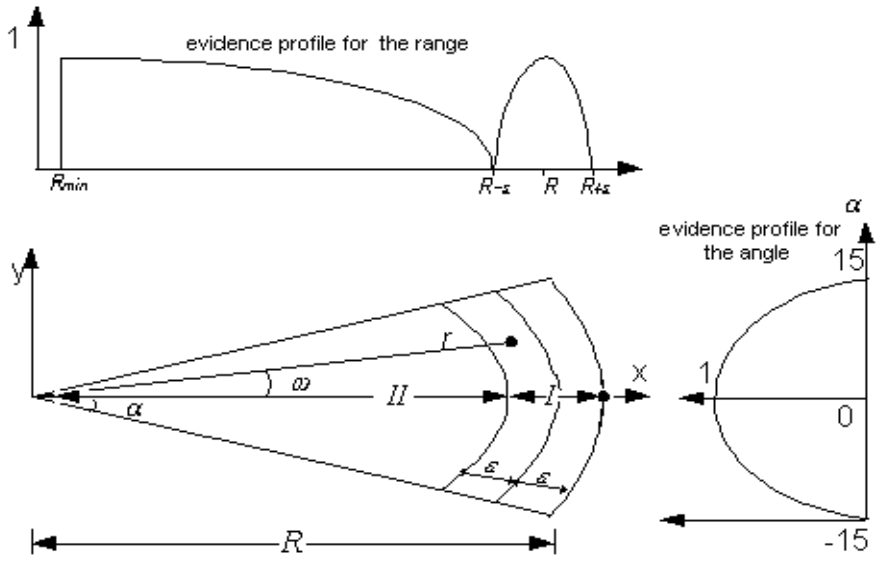

Region I: $R - \epsilon \leq r \leq R + \epsilon$, $-15^o \leq \alpha \leq 15^o$

Region II: $R_{min} \leq r < R - \epsilon$, $-15^o \leq \alpha \leq 15^o$

Figure 4.8: Sonar model, α is the half opening angle for a given sonar response R. $(r, \omega), -15^o$ □ ω □ 15^o, is a cell inside the sonar cone.

grids inside region I of Figure 4.8, it is reasonable to assume the nearer the cell is to the point $(R, 0)$ on the cone axis, the more evidence there is for the cell being *occupied*. If the cell is in region II, since a response from an object means the area between the sonar and the object should be empty, so the more nearer a cell is to the sonar inside the sonar cone, the more evidence there is for the cell being *empty*. Therefore the sonar model should be a function of the polar coordinates of the cell,

r and ω. The rest of the areas are assumed to be not sensed by the sonars, thus no evidence for either being *empty* or *occupied*.

Region I, where $R - \epsilon \square r \square R + \epsilon$:

$$m(\{occupied\}) = w_a(\frac{\alpha - \omega}{\alpha})^2 + w_r(\frac{\epsilon - |R - r|}{\epsilon})^2 \quad (4.7)$$

$$m(\{empty\}) = 0.00 \quad (4.8)$$

$$m(\{unknown\}) = 1.00 - m(\{occupied\}) \quad (4.9)$$

Region II, where $R_{min} \square r < R - \epsilon$:

$$m(\{occupied\}) = 0.00 \quad (4.10)$$

$$m(\{empty\}) = w_a(\frac{\alpha - \omega}{\alpha})^2 + w_r(\frac{R - \epsilon - r}{R - \epsilon})^2 \quad (4.11)$$

$$m(\{unknown\}) = 1.00 - m(\{empty\}) \quad (4.12)$$

R_{min} is the shortest range that the sonar can detect. In the case of our experiments, $R_{min} = 15cm$. ϵ is an error factor of the sonar response R. It represents how big the region I should be, where sonar response gives evidence only to cell's being *occupied*. The larger the ϵ is, the more cells in side the cone will be updated with evidence of being *occupied*. This is a conservative case since fewer cells would have high evidence for being *empty* in evidence grids. The robot would then navigate in a smaller area. Weight factors w_r and w_a are used to balance the effect of the range and angle. They are defined as,

$$w_r + w_a = 1 \quad (4.13)$$

According to Equation (4.13), the increase in one will cause the decrease in the

other. w_r and w_a balance the evidence distribution on radius and angle. In our experiments, we have set $w_r = w_a$ to obtain an average evidence distribution on both radius and angle. Figure 4.9 $\sim$ Figure 4.11 are examples of the sonar model projections on the evidence grids.

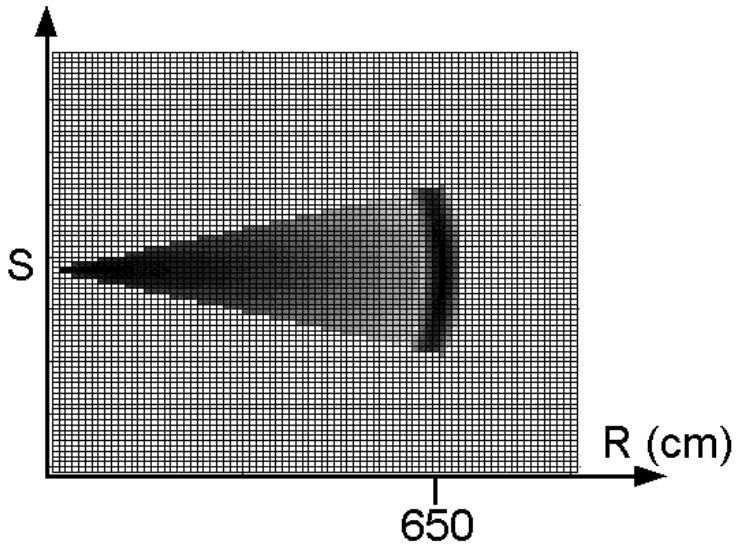

Figure 4.9: Example of sonar model projection on the evidence grids for being *unknown*. S is the ultrasonic sensor position. In the example, the sonar response $R = 650$cm. The *whiter* the cell is, the *higher* evidence there is for the cell being *unknown*.

These example figures were produced when $R = 6.5$m. The evidence distributions for cells being *occupied, empty, unknown* are represented in the tone distribution in these figures. In Figure 4.9, darker cells have higher evidence for being *unknown* while in Figure 4.10, the whiter cells have higher evidence for being *occupied*. Figure 4.11 show whiter cells having higher evidence for being *empty*.

In attempting to reduce unreliable readings caused by specular reflections, new methods have been derived by modifying the above ultrasonic sensor model. In the next chapter, discussions on dealing with specular reflections are given and experimental results are presented to show the effectiveness of the proposed new

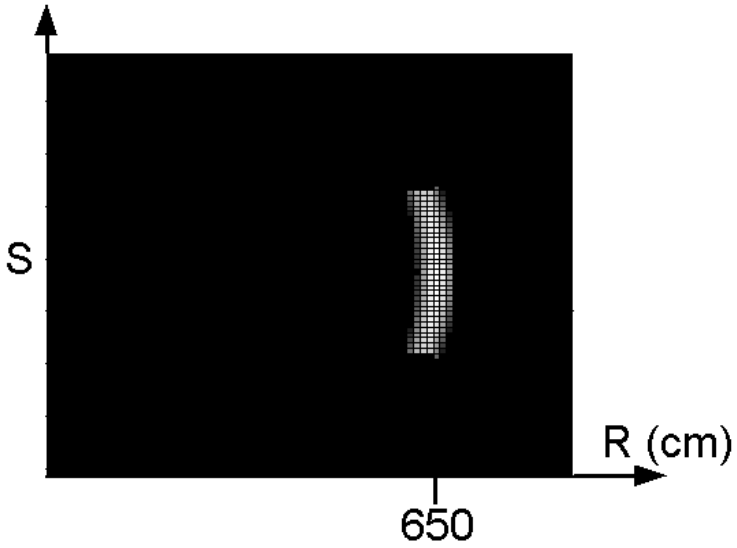

Figure 4.10: Example of sonar model projection on the evidence grids for being *occupied*. S is the ultrasonic sensor position. In the example, the sonar response $R = 650$cm. The *whiter* the cell is, the *higher* evidence there is for the cell being *occupied*.

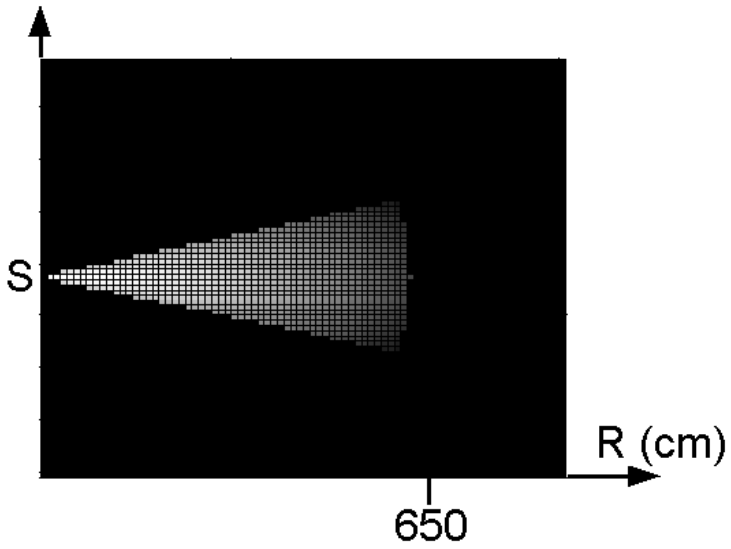

Figure 4.11: Example of sonar model projection on the evidence grids for being *empty*. S is the ultrasonic sensor position. In the example, the sonar response $R = 650$cm. The *whiter* the cell is, the *higher* evidence there is for the cell being *empty*.

methods.

Chapter 5

Dealing with Specular Reflections

5.1 Range Confidence Factor

5.1.1 More Discussions on Specular Reflections

The physical reasons of specular reflection have been described in Chapter 4. All raw sensor responses are projected onto the grid using the sensor model. The sensor model given in Equation (4.7)∼Equation (4.12) was deduced from the sonar profile introduced in [26, 3]. It is effective in converting range information of ultrasonic sensors into evidential information to be fused on evidence grids. The model has taken the angular error into account by using a probability distribution function. But the model does not take specular reflection into consideration. The specular reflection is a very serious problem particularly in confined environments [19]. Specular reflections cause unreliable ultrasonic responses. These sonar responses are indiscriminately taken as reliable ones for the sensor fusion purpose. This consequently affects the accuracy of the grid map produced.

Since the sonar response is to be projected onto the grid, it is reasonable to lower the confidence for those sonar readings which are suspected to be caused by specular reflections. Specular reflections cause longer sonar responses since the sonar signals may be reflected off several surfaces. Therefore, we can interpret the longer range information as less believable than the shorter ones. Thus the unreliable readings will be accorded with a reduced confidence. The downside of this measure is that the evidence accumulating process will be slowed down consequently.

5.1.2 The Range Confidence Factor

A special adjusting term called *range confidence factor, RCF*, has been used for dealing with specular reflections. The idea of RCF was first introduced in [42]. The RCF is defined as,
when $R > R_{max}$:

$$RCF = RCF_{min} = \frac{R_{Th}}{R_{Th}+1} \tag{5.1}$$

when R □ R_{max}:

$$RCF = \frac{(\frac{R_{max}-R}{R_{max}})^{\tau} + R_{Th}}{1+R_{Th}} \tag{5.2}$$

where R is the ultrasonic sensor response, τ is a controlling constant for RCF, R_{Th} is the threshold value of R, and R_{max} is the maximum R value for RCF. RCF_{min} is the lowest value that RCF would have. The RCF is applied by simply multiplying it with Equation (4.7) and Equation (4.11) as,

$$m(\{occupied\}) = RCF \times [w_a(\frac{\alpha - \omega}{\alpha})^2 + w_r(\frac{\epsilon - |R - r|}{\epsilon})^2] \quad (5.3)$$

$$m(\{empty\}) = RCF \times [w_a(\frac{\alpha - \omega}{\alpha})^2 + w_r(\frac{R - \epsilon - r}{R - \epsilon})^2] \quad (5.4)$$

RCF is determined by three parameters, τ, R_{th} and R_{max}. RCF_{min} is the lowest value that RCF can have. RCF_{min} depends on R_{Th}. Equation (5.1) sets a constant RCF_{min} whenR_{th} is fixed. Therefore, the threshold value R_{Th} sets the lower limit of RCF. In our experiments we have set $RCF_{min} = 0.1$, corresponding to $R_{Th} = \frac{1}{9}$. Equation (5.2) shows that RCF approaches RCF_{min} when R approaches R_{max}. R_{max} is a threshold value which shows the confidence of the maximum range detection of sonar in a certain environment. Hence, for a small R_{max}, RCF approaches RCF_{min} more rapidly.

τ is used to reflect the sensitivity of the sensor to the reflected specular signal [42]. Therefore, τ reflects the environment features. The value of τ also controls how fast the RCF can approach the RCF_{min} for a certain range response R. Figure 5.1 shows two sets of RCF curves with different τ values. In Figure 5.1a where $\tau < 1$, RCF decreases more slowly than it does in Figure 5.1b, where $\tau > 1$. Figure 5.1 further shows that the larger the τ is, the smaller the value of RCF will be when the range response is less than R_{max}. When the range response R is larger than R_{max}, RCF is restricted to the constant RCF_{min}.

For a numerical example, when $R_{max} = 6.5m$ and $RCF_{min} = 0.1$, with τ given as 2, RCF becomes a function of the ultrasonic sensor response R only. For any response R shorter than $R_{max} = 6.5m$, RCF changes according to the curve $\tau = 2$ in

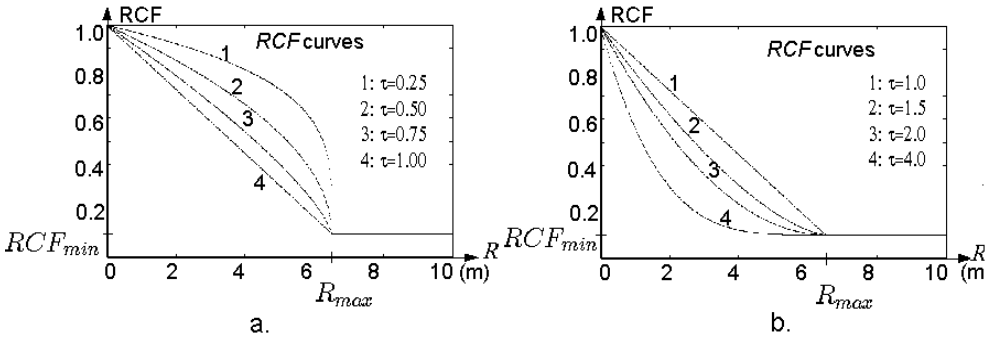

Figure 5.1: Example curve of RCF with different τ. a. τ □ 1 and b. $\tau \geq 1$.

Figure 5.1a. Whenever there is a response $R > R_{max} = 6.5m$, RCF will be limited to the threshold RCF_{min}. The parameters τ, R_{max} and R_{min} are set by trial and error. From our experiments, we have found $\tau = 2$, $R_{max} = 6.5m$ and $R_{min} = 0.1$ are satisfactory.

The RCF is actually a discounting factor which adjusts the evidence for grid cells as shown in Equation (5.3) and Equation (5.4). The closer the sonar response R is to R_{max}, the lower RCF it has. When the sonar response R exceeds R_{max}, it has the lowest RCF which is RCF_{min}. For different sonar responses, evidence produced have been discounted by their corresponding RCFs. For those unreliable readings caused by specular reflections, as discussed in the earlier section, they are much longer than they should be. Therefore, their corresponding RCFs are much lower. Hence, when RCF is applied as shown in Equation (5.3) and Equation (5.4), unreliable responses affected by specular reflections will produce less evidence. This consequently avoids accumulating evidence for unreliable sensory information caused by specular reflections.

5.1.3 Experimental Results

The effect of RCF in accounting for unreliable readings has been tested in a confined environment in our laboratory. The sensor fusion algorithm used to produce the grid map was based on Dempster-Shafer's method introduced in Equation (3.27) $\sim$ Equation (3.29), Section 3.4. The overview of the testing environment is given in Figure 5.2. Ultrasonic sensor data were collected at known positions within the environment. Arbitrarily 30 positions were selected within the testing environment. Boundaries of this testing environment were made of plywood and carton. Nomad Super Scout II with a 16-sonar sonar ring was used for collection sensor responses. All the 16 ultrasonic sensors were fired at each of these 30 positions and data were collected. Then the sensor fusion based on the modified sensor model given in Equation (5.3) and Equation (5.4) was done offline.

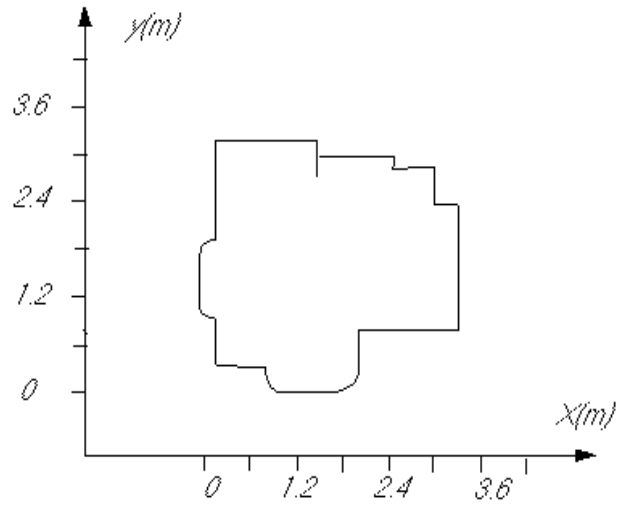

Figure 5.2: The confined environment for testing the effectiveness of RCF. Boundaries of this environment were made of plywood and carton. Nomad Super Scout II with a 16-sonar sonar ring was used for sensory data collection.

Figure 5.3 $\sim$ Figure 5.7 present experimental results of evidence for cells being

occupied on the 2D evidence grids. 30 fixed positions were selected beforehand for Super Scout II to collect the ultrasonic sensor data from the 16-sonar sonar ring. All figures shown have been thresholded to give a better view. Figure 5.3 shows evidence grids when the RCF was not applied. Uncertainties in this figure are obvious and are particularly pronounced in areas near corners and arcs. When the RCF was

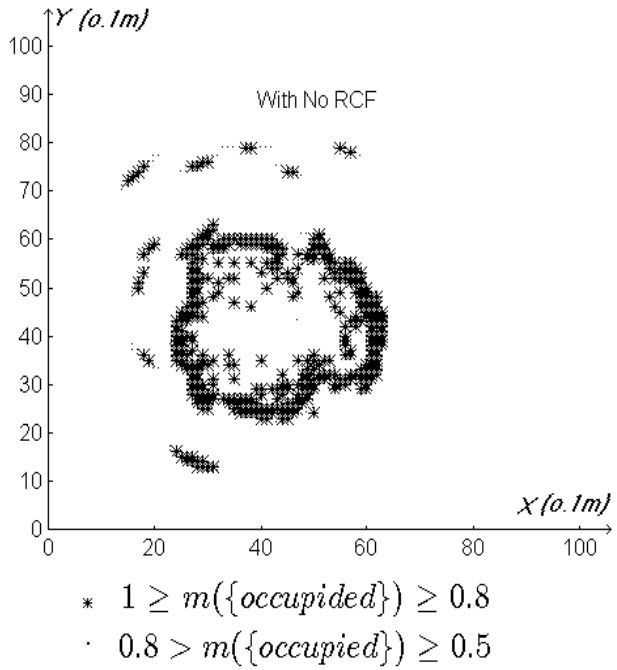

Figure 5.3: Evidence for being *occupied* without using RCF in the sensor model.

used to modify the sensor data, these unreliable readings were reduced dramatically as shown in Figure 5.4 $\sim$ Figure 5.7. These results also show how different selections of the three parameters in Equation (5.2) could bring about different effects.

Figure 5.4 $\sim$ Figure 5.7 prove that RCF does work well in reducing the unreliable responses shown typically in Figure 5.3. However whether RCF can best perform depends highly on the selection of parameters in Equation (5.2). RCF acts as a discounting factor in reducing unreliable responses. The price to pay for the improvement of sensor responses is the decreased rate of evidence accumulation

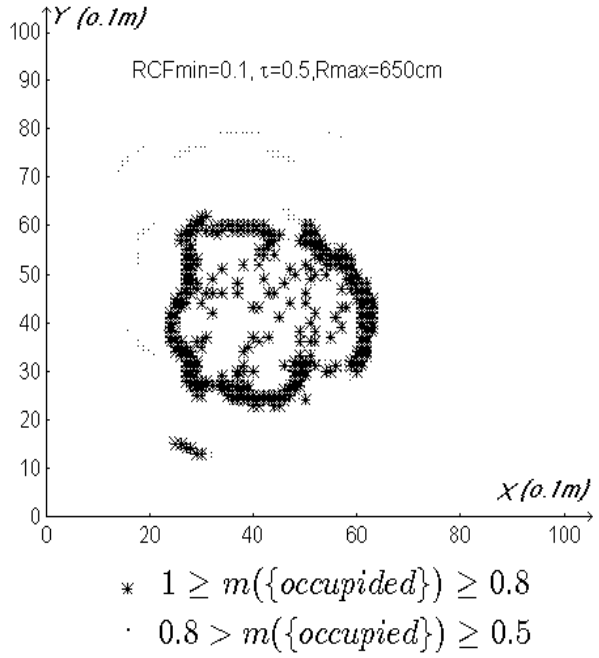

Figure 5.4: $RCF_{min} = 0.1, \tau = 1.5, R_{max} = 500cm$

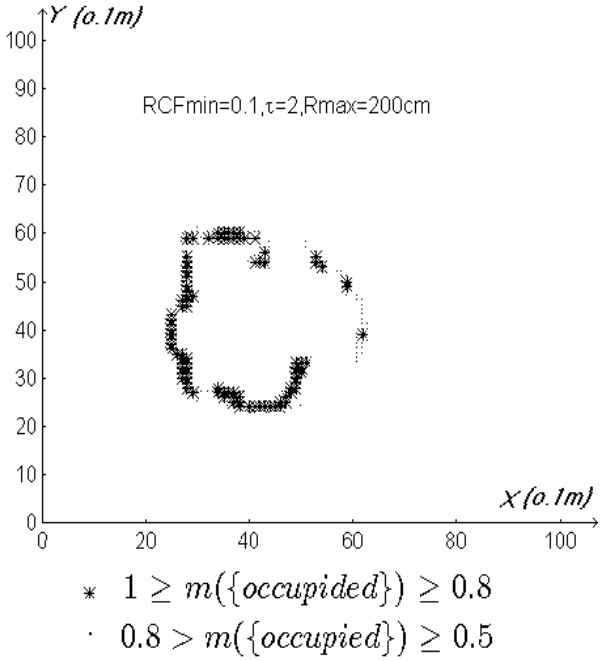

Figure 5.5: $RCF_{min} = 0.1, \tau = 0.5, R_{max} = 650cm$

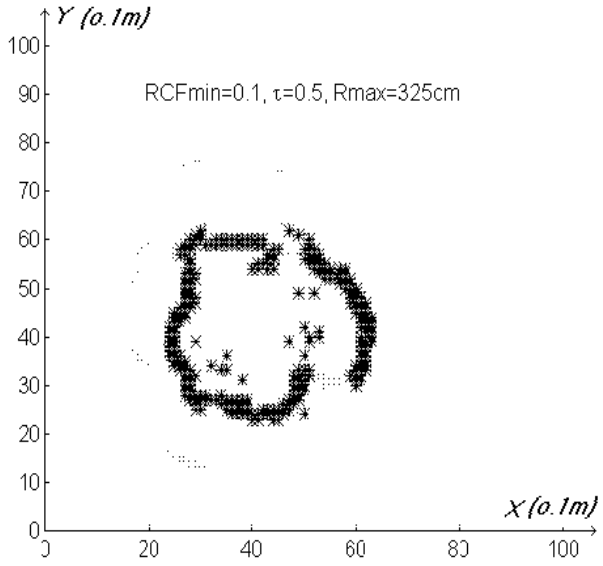

$*$ $1 \geq m(\{occupided\}) \geq 0.8$

$\cdot$ $0.8 > m(\{occupied\}) \geq 0.5$

Figure 5.6: $RCF_{min} = 0.1, \tau = 0.5, R_{max} = 325cm$

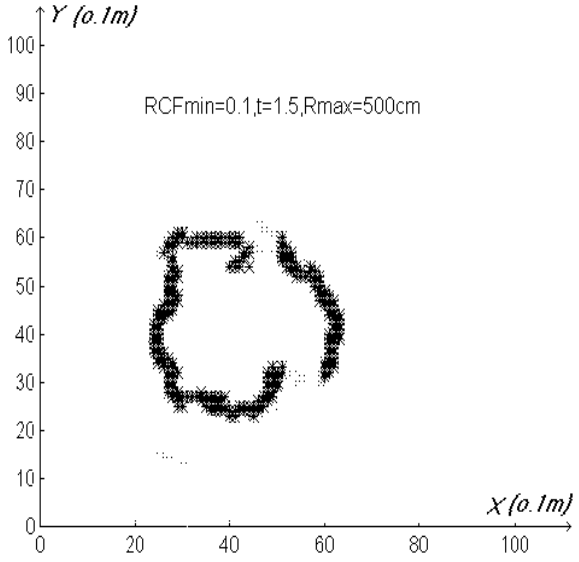

$*$ $1 \geq m(\{occupided\}) \geq 0.8$

$\cdot$ $0.8 > m(\{occupied\}) \geq 0.5$

Figure 5.7: $RCF_{min} = 0.1, \tau = 2, R_{max} = 200cm$

because of the filtering effect due to RCF. This is so as RCF will discard those sonar responses which are thought to be due to specular reflections. However they may also contain information that is actually useful. This can be compensated for by increasing the number of sets of sensor readings at more robot locations.

The sharp difference between Figure 5.4 and Figure 5.5 arises from the two extreme cases in the experiments. In Figure 5.4, the sensor model was assigned the much more conservative set of parameters for RCF than it was in Figure 5.5. Obviously the sensor model parameters chosen for Figure 5.5 was much better in reducing unreliable responses as compared to the parameters chosen for Figure 5.4. However as also shown in Figure 5.4, a rather great amount of information has been lost as well. Figure 5.6 was just a case of in-between comparing with Figure 5.4 and Figure 5.5. Among these figures, Figure 5.7 shows the best set of parameters that have successfully reduced unreliable readings while incurring relatively little loss of information. Therefore, to find an effective set of parameters to produce the most satisfactory RCF is of great importance in applying RCF. In our experiments, the selection of the three parameters is very much a trial and error process.

5.2 Adaptive Sensor Model

5.2.1 Using Confidence Value for Adaptive Sensor Model

We have shown that RCF worked very well in reducing unreliable sensor readings caused by specular reflections in sensory information as discussed in the previous section. These results were presented in our paper [93]. However, to set parameters beforehand for RCF is obviously impractical as the mobile robot is to navigate in unknown environments. We have also noticed that inappropriate selection of

parameters could result in unsatisfactory performance of RCF as shown in Figure 5.4.

Noticing that the term □ in Dempster-Shafer's evidence theory directly reflects how much the different sources of evidence are in conflict with each other, we proposed using the term □ to adjust the RCF dynamically. In our case, for two sources of evidence, the new evidence from the sensor and the old evidence in grids, □ is given by,

$$□ = \sum_{X \cap Y = \phi} m_n(X) m_o(Y) \tag{5.5}$$

Specular reflections cause much larger range readings than they should be. When specular reflections happen at a position, the conflict between the evidence from this unreliable reading and the existing evidence could be treated as an indicator. This indicator reflects the reliability of the ultrasonic sensor reading. Since RCF is a discounting factor to adjust the evidence from the new sensor reading, we can use the conflict value to help select the appropriate value for RCF. Hence, the conflict value can be used to set parameters of RCF continuously during the sensor fusion process. When the conflict value is rather high, it means the new evidence from sensors is quite different from the existing evidence. Therefore, the high conflict shows most probably there has been a false reading from the ultrasonic sensor caused by specular reflections. Based on this consideration, the following factor denoted as Ω has been introduced to the sensor model. Ω is defined as,

$$\Omega = (\frac{1 - □}{1 + □})^2 \tag{5.6}$$

The relationship between Ω and □ is shown in Figure 5.8. The application of Ω in the

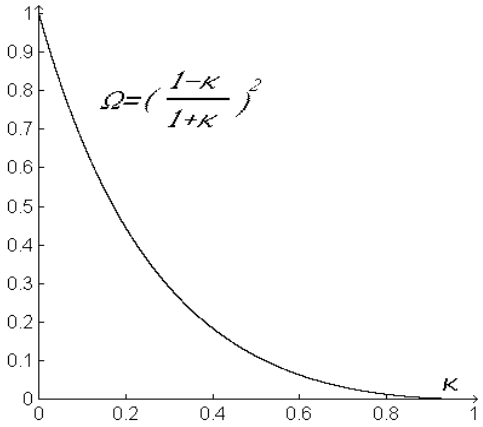

Figure 5.8: Relationship between Ω and □, Ω is in y-axis and □ in x-axis

following equations will change the parameters of RCF accordingly. For Equation (5.2), we modify the τ and R_{max} as,

$$\tau' = \frac{1}{\Omega} = (\frac{1+\square}{1-\square})^2 \tag{5.7}$$

$$R'_{max} = R_{max} \cdot \Omega = R_{max} \cdot (\frac{1-\square}{1+\square})^2 \tag{5.8}$$

Since R_{max} is adjusted continuously in the sensor fusion process as shown in Equation (5.8), there is no need for us to know the environmental information beforehand to set R_{max} now. This is more practical for navigating in unknown environments. R_{max} then can be as the longest range reading of the ultrasonic sensor. In our case, we have set it to 6.5m, which is the longest range reading reported by the ultrasonic sensing unit in the Nomad Super Scout II mobile robot. The modified RCF is denoted as RCF',

when $R > R'_{max}$:

$$RCF' = RCF_{min} \quad = \quad \frac{R_{Th}}{R_{Th}+1} \tag{5.9}$$

when $R \square R'_{max}$:

$$RCF' = \frac{(\frac{R'_{max}-R}{R'_{max}})^{\tau'} + R_{Th}}{1 + R_{Th}} \tag{5.10}$$

With modifications introduced in the above equations, the sensor model will automatically adjust RCF according to the change in the conflict value. To apply this method, Equation (4.7) and Equation (4.11) are now modified as,

$$m(\{occupied\}) = RCF' \times [w_a(\frac{\alpha-\omega}{\alpha})^2 + w_r(\frac{\epsilon-|R-r|}{\epsilon})^2] \tag{5.11}$$

$$m(\{empty\}) = RCF' \times [w_a(\frac{\alpha-\omega}{\alpha})^2 + w_r(\frac{R-\epsilon-r}{R-\epsilon})^2] \tag{5.12}$$

5.2.2 Experimental Results

The effect of the new adaptive model is shown in Figure 5.9 and Figure 5.10 in the same environment for the same robot as in section 5.1. The conflict is calculated between the evidence from new the sensor reading and those existing one. The old evidence will not be updated if the new $\square$ is large enough to discard the new sensor response.

Results of the new method in Figure 5.10 showed the effectiveness of the adaptive sensor model with the application of the modified RCF given in Equation (5.9) . This has provided us a new approach to improve the accuracy of robot's knowledge about its environments. The most outstanding advantage that comes with this approach is that no *a priori* environmental knowledge for R_{max} will then be needed.

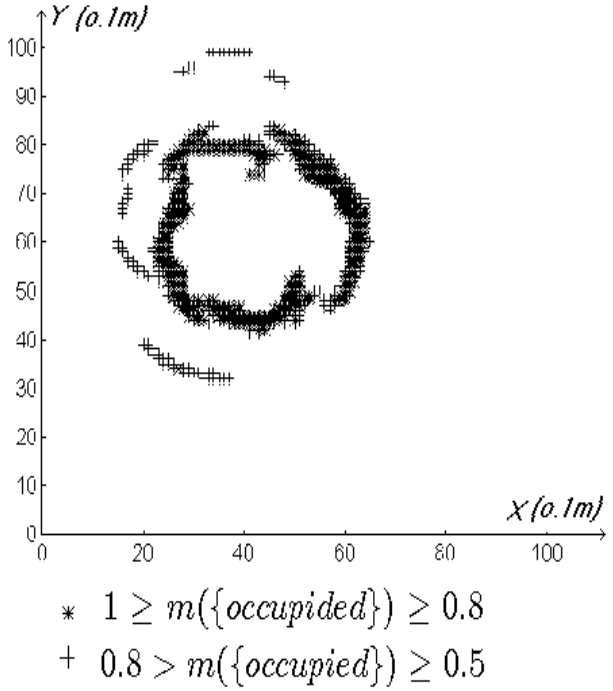

Figure 5.9: When Ω was not applied to RCF.

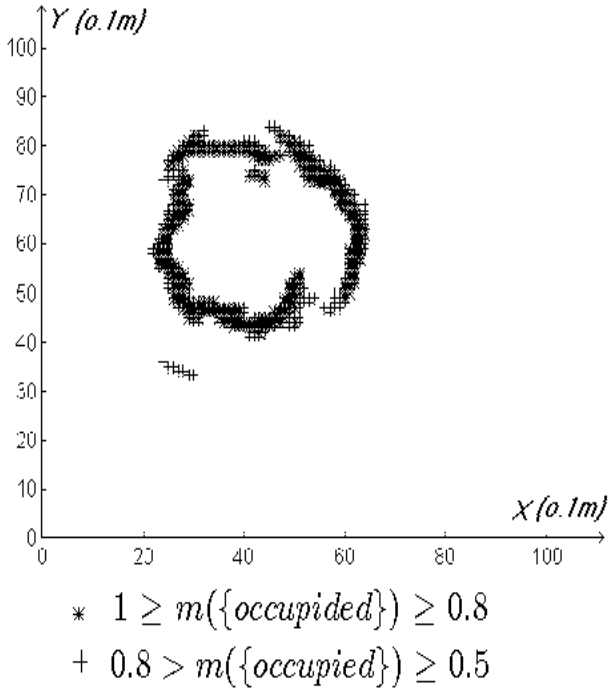

Figure 5.10: When Ω has been applied to RCF.

5.3 Outlier Rejection Algorithm

In this section, a simple algorithm called *outlier rejection algorithm (ORA)* has been derived to be used together with the adaptive sensor model proposed in the last section. The *ORA* was especially useful in canceling those unreliable readings in the outlying areas of the actual environment boundaries.

5.3.1 Algorithm Details

Outlying areas of an environment are actually irrelevant to the mobile robot. It is likely that these areas are only updated by the sensor updating process a few times in each round of sensor scan. These updatings are not from reliable sensor readings as they are actually beyond the sensing range of ultrasonic sensors. Their existence probably is due to specular reflections. An *outlier rejection algorithm (ORA)* is introduced to reject the unreliable evidence in these outliers and to improve the reliability of the overall accumulated evidence. The algorithm relies on checking the number of times that a particular cell has been updated in every sensor scan. For a cell at (i, j), we define,

$$\mu_{(i,j)} = number\ of\ updatings \tag{5.13}$$

where i=1,..,$GridsMapLength$; j=1,...,$GridsMapWidth$. $GridsMapLength$ and $GridsMapWidth$ are the maximum length and width of the evidence grids. The *Outlier Rejection Algorithm* will then compare $\mu_{(i,j)}$ with a threshold value called *critical updated times*, denoted as $\overline{\mu}$. If $\mu_{(i,j)} < \overline{\mu}$, the cell is then rejected or treated as a cell with "*unknown*" evidence by resetting its evidential values in accordance to Equation (3.23) $\sim$ Equation (3.25), Section 3.4. The selection of $\overline{\mu}$ was through

a trial-and-error process in experiments. Based on the original sensor fusion process given in Figure 3.2, the implementation of this algorithm is shown in Figure 5.11.

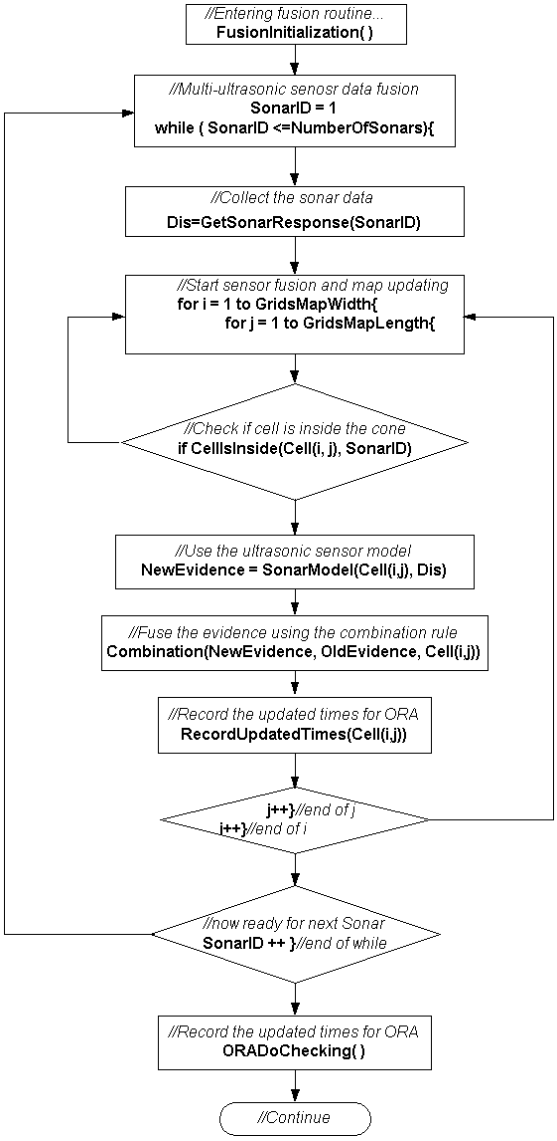

Figure 5.11: Flow diagram for the multi-ultrasonic sensor fusion process with ORA implementation.

5.3.2 Experimental Results

The algorithm has been tested in a new typical confined environment in our laboratory. The following figure gives the overview of this environment. Boundaries of this environment are made of plywood and carton. Nomad Super Scout II with a 16-sonar sonar ring was used for sensory data collection. $\overline{\mu}$ in the experiments was set as 4. Figure 5.13 $\sim$ Figure 5.20 present all experimental results of fused evidence for *occupied* cells on 2D evidence grids.

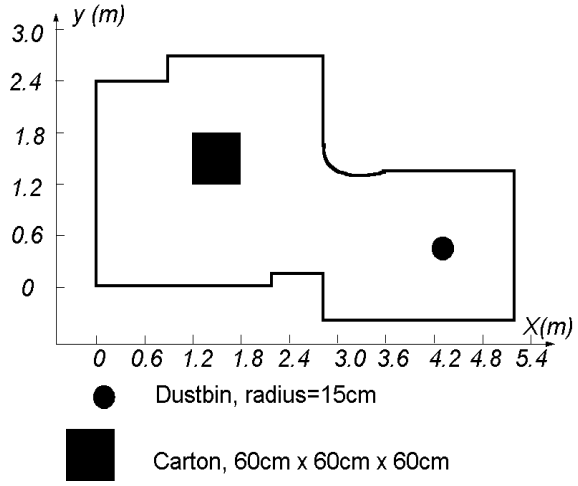

Figure 5.12: A typical confined environment with 2 objects inside. Boundaries of this environment are made of plywood and carton. Nomad Super Scout II with a 16-sonar sonar ring was used for sensory data collection.

Figure 5.13 $\sim$ Figure 5.16 were experimental results of the *Outlier Rejection Algorithm* in the environment given in Figure 5.12 without any objects inside. 28 fixed positions were selected beforehand for Super Scout II to collect the ultrasonic sensor data from the 16-sonar sonar ring.

With the adaptive sensor model, evidence from unreliable readings were reduced considerably in Figure 5.14 as compared with Figure 5.13. With the introduction of ORA, we found that the algorithm worked very well for eliminating ultrasonic

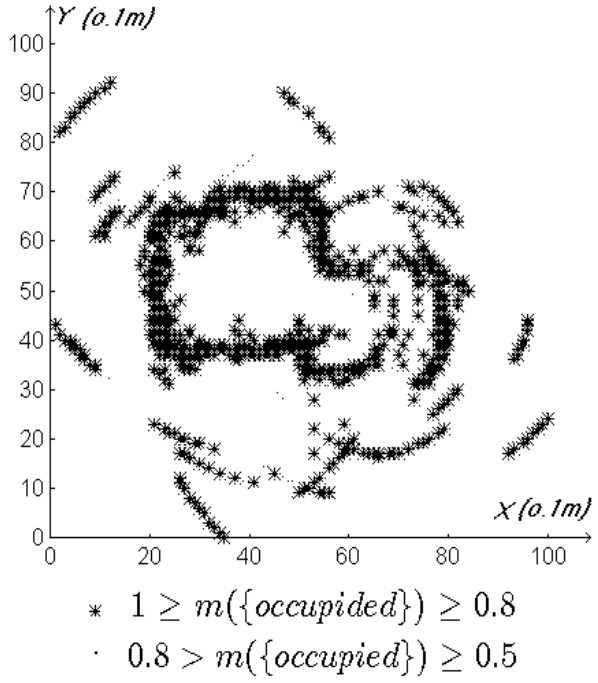

Figure 5.13: Using sensor model without RCF.

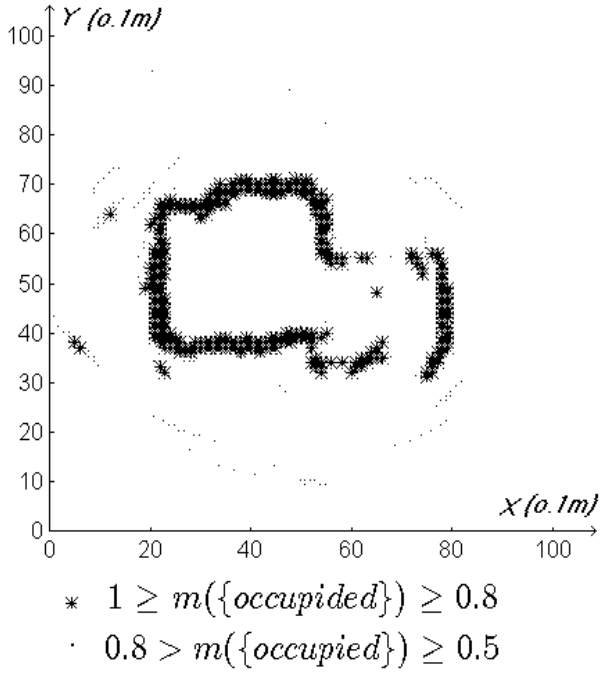

Figure 5.14: Using sensor model with the adaptive RCF.

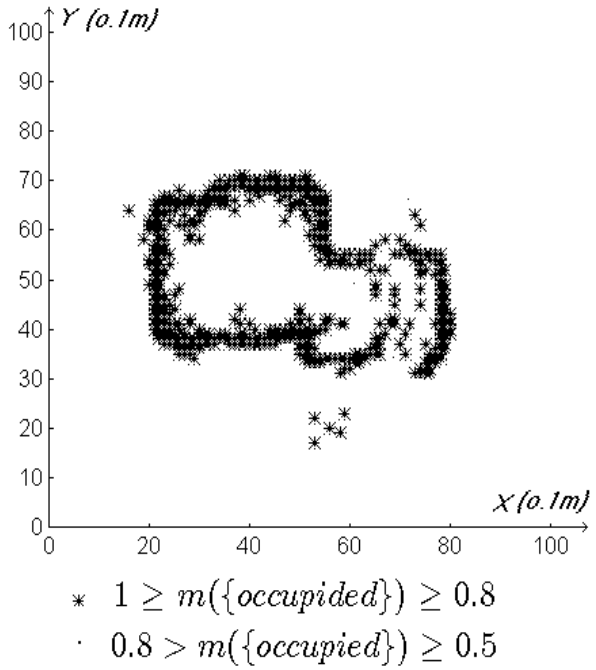

Figure 5.15: Using sensor model without RCF but with the ORA .

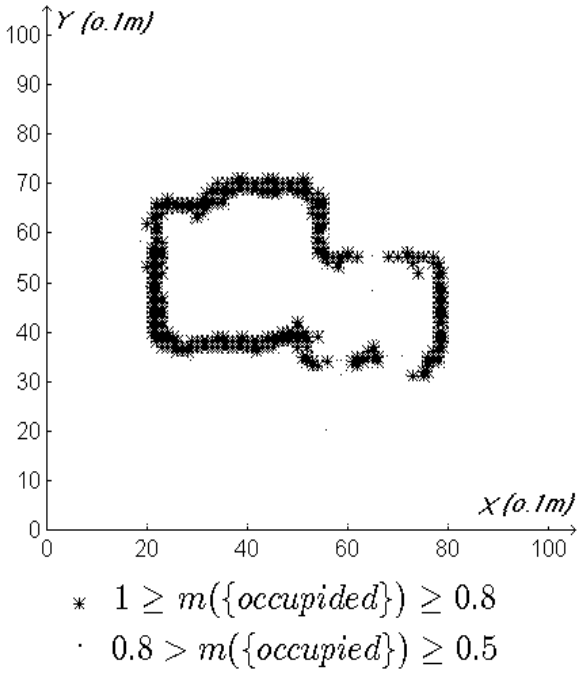

Figure 5.16: Using both the adaptive sensor model and ORA.

responses from those outlying areas that are actually beyond the detection of ultrasonic sensors. This is shown in Figure 5.15 and Figure 5.16. In the case of those cells whose evidence has been corrupted by specular reflections, these cells were updated only for a limited number of times during the various scans of the robot. They actually remain *unknown* at most of other time. The state of such cell changes abruptly from a high probability of being occupied to a high probability of being empty or vice versa. This confirms what we have discussed in Section 5.3.1. The limited times of updatings caused by the specular reflections still resulted in rather high evidence assignment to these cells. The ORA successfully resets the evidence of these cells as *unknown* according to Equation (3.23) $\sim$ Equation (3.25) because they are actually not relevant to the robot. But we also notice ORA should work together with the adaptive sensor model to guarantee a better performance as shown in Figure 5.16.

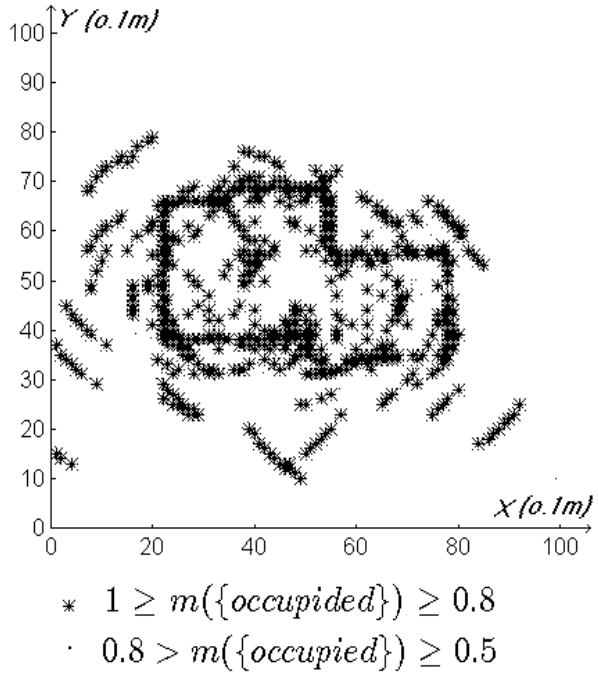

Figure 5.17: Using the sensor model without RCF.

Figure 5.17 $\sim$ Figure 5.20 present experimental results in the same testing envi-

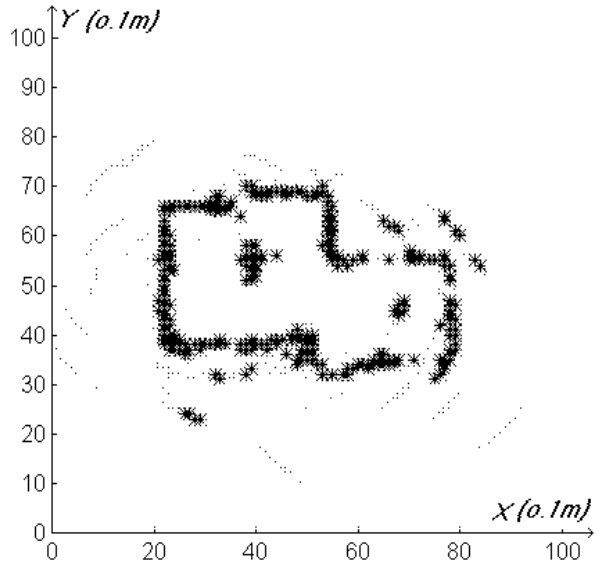

Figure 5.18: Using the adaptive sensor model only.

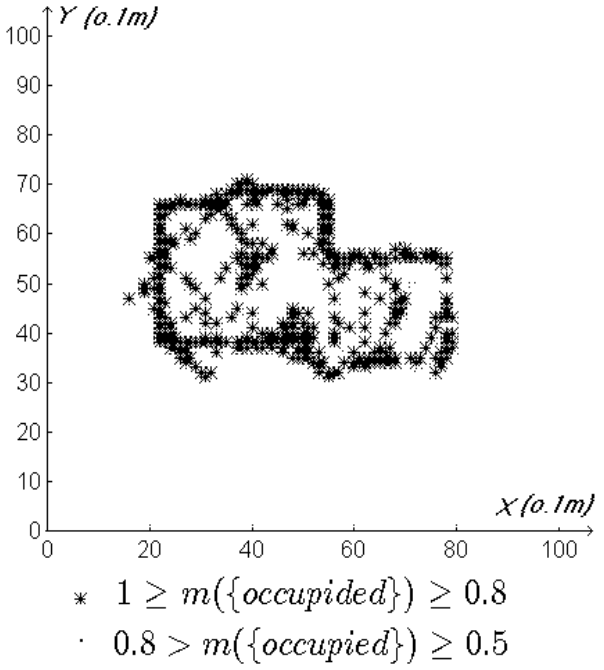

Figure 5.19: Using the ORA only.

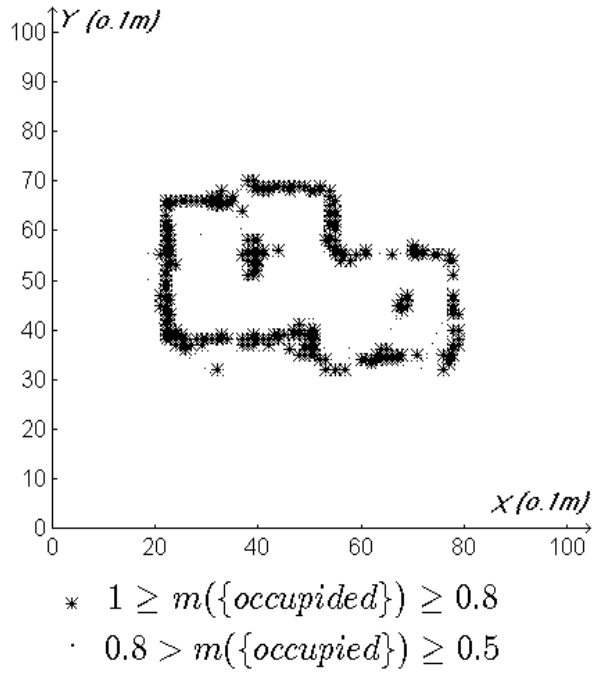

Figure 5.20: Using both the adaptive sensor model and *ORA*.

ronment in Figure 5.12 with 2 objects inside. In this case, 25 fixed positions were selected beforehand for Super Scout II to collect the ultrasonic sensor data from the 16-sonar sonar ring.

In the results, the effectiveness of *ORA* can still be seen. However, we have also noticed that the problem of specular reflections in Figure 5.17 was much more serious than it was in Figure 5.13. This is due to the objects inside the environment.

From the experimental results, again we noticed that in the first place, instead of being used alone, *ORA* should be used in combination with the adaptive sensor model. As shown in Figure 5.19, when only *ORA* was applied, it appeared ineffective in dealing with specular reflections. But, after adaptive sensor model has been used together with *ORA*, as shown in Figure 5.20, both outlier and inside unreliable readings in Figure 5.17 have been overcome considerably. Figure 5.16 and Figure 5.20 proved this as they present satisfactory results in reducing unreliable readings.

We have also noticed that ORA is needed because the outlier readings can be reduced greatly through this simple algorithm. These outlier readings are not easily removed by RCF or RCF' since they have less conflict. Therefore, it is necessary to apply ORA to the adaptive sensor model with RCF' to obtain the best experimental results. With the proposed sensor model which is able to reduce unreliable sensor responses caused by specular reflections, the accuracy of the grid map produced can be improved greatly.

Chapter 6

Dead Reckoning for Localization and Path Planning

Based on the grid map that has been established by the multi-ultrasonic sensor fusion algorithm in the map-building process, the robot is now ready to navigate autonomously. In experiments discussed in Chapter 3, Chapter 4 and Chapter 5, to test the correctness of our algorithms, we depended on the known positional information of the robot. Therefore sensory information collected at known positions was fused by offline calculation. Then in Chapter 6 our algorithms were used to the real-time robot navigation. In these experiments, the positional information was derived from dead reckoning. Localization errors were accumulated during the experiment progress, correction should be made on the positional information from dead reckoning, correction should be made on the positional information from dead reckoning. To meet this purpose, an error compensation algorithm is introduced to do the continuous compensation for dead reckoning errors. To navigate, the robot needs to know where it is to go. This is accomplished by a path planning algorithm.

The path planning algorithm attempts to find an appropriate path through empty areas of the environment to reach the goal. In this chapter, a dead reckoning error correction algorithm for localization and a path planning algorithm are presented.

6.1 Dead Reckoning Errors

Whenever a robot moves, accurate positional information must be fed to the system. The robot needs to know its current location for map updating and navigation [39]. There are several methods to deal with the localization problem for a sonar-based robot [50]. These include using Kalman filtering to update the orientation and position [43], feature extraction from the grid map as landmarks [11], direct grid map matching for continuous localization [9], and dead reckoning for localization [39]. Dead reckoning technique has been used in this project for its simplicity [9, 14, 27]. However, due to errors accumulated in the navigation process [39], using only dead reckoning for localization is not sufficient. According to [35, 40], for *wheeled mobile robots (WMR),* there are two categories of sources in dead reckoning errors, the *systematic errors* and the *non-systematic errors.* They are due to several reasons as:

- Systematic errors are due to:
  - Unequal wheel diameters
  - Average of actual wheel diameters differs from nominal wheel diameter
  - Actual wheelbase differs from nominal wheelbase
  - Misalignment of wheels
  - Finite wheel encoder resolution

  - Finite encoder sampling rate

- Non-systematic errors are due to:

  - Traveling over uneven floors
  - Traveling over unexpected objects
  - Wheel slippage

For the two categories of errors, systematic errors are particularly important because they accumulate continuously. The robot in this project has been aimed to be used in confined spaces such as toilets and offices. For navigation in these confined environments, systematic errors are much more dominant than non-systematic errors. The error correction algorithms developed are meant to reduce systematic errors.

6.1.1 Error Calibration

The robot platform used in our experiments is a Nomad Super Scout II mobile robot. Specifications are included in Appendix B. The Super Scout II robot is a wheeled mobile robot (WMR). There are two differential drives. The encoder resolution for translation is 756 counts/cm and for rotation is 230 counts/degree. In the calibration, the dimension testing paths was small as our robot is expected to perform its tasks in a small confined space [87].

To do the calibration of translation error, the mobile robot was programmed to travel in 3 straight paths for different lengths. The translation error was the difference between the actual distance traveled and the desired distance. Distances of 200cm, 254cm and 300 cm were used and each was repeated for 10 times. Errors of each time were recorded and finally averaged to obtain the translation error [87].

To measure the orientation error, the robot was programmed to travel in 3 square paths of different sizes in both clockwise and anti-clockwise directions. The orientation error was calculated from the differences of the robot's start position and the end position. The dimension of the 3 square paths were a 200cm×200cm, 254cm×254cam and 300cam×300cm. In each path, measurement was done repeatedly for 10 times and the error was then obtained by calculating the average value [87].

The final results of both translation error and orientation errors obtained are shown in table 6.1.

Translation Error E_t	**Clockwise Error** E_{cw}	**Counter-Clockwise Error** E_{ccw}
5.3 mm	1.1932861^o	$0.7658235\ ^o$

Table 6.1: Calibrated errors in translation and orientation of Super Scout II mobile robot.

After the error calibration, mathematical models for error correction were derived base on the calibration results. This is discussed in the next section.

6.1.2 Error Compensation Algorithms

Error compensation process is done based on the calibrated errors obtained in the previous section. As shown in Figure 6.1, there are 3 modules in the compensation process, compensation for the translation error, compensation for the clockwise rotation error and compensation for the counter-clockwise rotation.

The algorithm to compensate the translation error is shown in Equation (6.1),

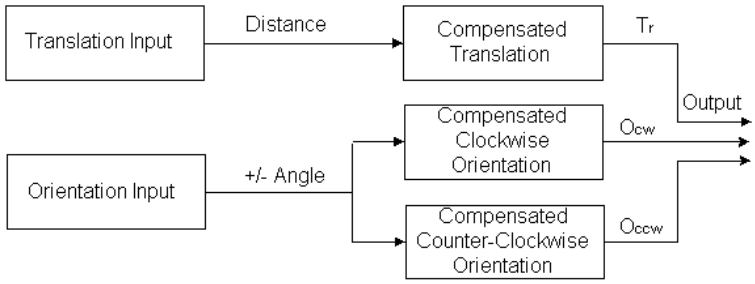

Figure 6.1: Block diagram of the error compensation process of the Nomad Super Scout II mobile robot.

where an exponential function has been used [87],

$$T_r = d - E_t \times (1 - e^{-(\frac{d}{\lambda})^{\rho}}) \tag{6.1}$$

where T_r is the adjusted distance of the robot, d is the programmed distance, E_t is the translation error to be compensated. λ and ρ are the two model parameters. From Table 6.1 E_t=5.3 mm = 2.086 in term of 0.1 inch. Since the Super Scout II robot uses 0.1 inch as translation unit, the calculation of parameters used 0.1 inch as unit in order to feed the results directly to the robot. Figure 6.2 shows the diagram for calculating the two parameters.

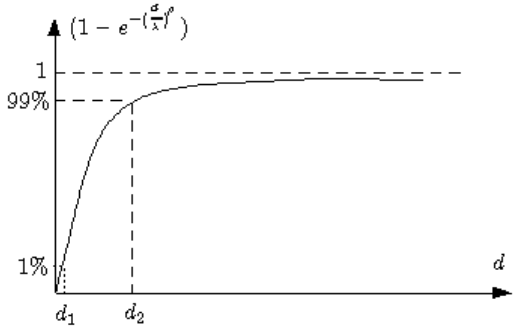

Figure 6.2: Calculating the parameters λ and ρ in the translation error compensation model.

In calculating λ and ρ from Figure 6.2, to obtain a very short rise time, we assumed that when d=d_1=2.54cm, it had reached 1% of the error, and when d=d_1=5.08cm, it had reached 99% of the error. To feed the value to the robot movement control, d_1 and d_2 were converted into $d_1 = 10$ and $d_2 = 20$ term of 0.1 inch. Therefore, using the following Equation (6.2), we obtain λ and ρ which are tabulated in Table 6.2.

$$\begin{cases} 0.01 = 1 - e^{-(\frac{d_1}{\lambda})^{\rho}} \\ 0.99 = 1 - e^{-(\frac{d_2}{\lambda})^{\rho}} \end{cases} \tag{6.2}$$

Parameter	λ	ρ
Parameter Values	16.82567822251	8.83986694952

Table 6.2: Parameters for translation compensation.

To compensate for the orientation error, a third-order model was used for both clockwise and counter-clockwise rotation. The model is given as,

$$y_i = \epsilon_1 \cdot x_i + \epsilon_2 \cdot x_i^2 + \epsilon_3 \cdot x_i^3 + err_i \qquad i = 1, \ldots, 10 \tag{6.3}$$

where x_i is the ith uncompensated input, y is the ith compensated output, err_i is the ith error to be compensated. ϵ_1, ϵ_2 and ϵ_3 are model parameters. Thus the least square error was,

$$\sum_{i=1}^{10} err_i^2 = \sum_{i=1}^{10} (y_i - \epsilon_1 \cdot x_i - \epsilon_2 \cdot x_i^2 - \epsilon_3 \cdot x_i^3)^2 \tag{6.4}$$

To obtain the minimum of Equation 6.4, it was differentiated and equated to zero

with respect to ϵ_1, ϵ_2 and ϵ_3. This is shown in Equation 6.5.

$$\begin{cases} -2\sum x_i \cdot (y_i - \epsilon_1 \cdot x_i - \epsilon_2 \cdot x_i^2 - \epsilon_3 \cdot x_i^3) = 0 \\ -2\sum x_i^2 \cdot (y_i - \epsilon_1 \cdot x_i - \epsilon_2 \cdot x_i^2 - \epsilon_3 \cdot x_i^3) = 0 \\ -2\sum x_i^3 \cdot (y_i - \epsilon_1 \cdot x_i - \epsilon_2 \cdot x_i^2 - \epsilon_3 \cdot x_i^3) = 0 \end{cases} \tag{6.5}$$

The calculation was done for both clockwise and counter-clockwise rotation. Final results are shown in Table 6.3 [87].

	ϵ_1	ϵ_2	ϵ_3
Clockwise	1.011667289565	0.00528547951	0.000484924056
Counter Clockwise	0.97648492884	0.007325616437	0.00066983573

Table 6.3: Parameters rotation error compensating model.

6.1.3 Testing Results of Dead Reckoning Error Compensation

Testing results on the error compensation algorithms are given in Figure 6.3 $\sim$ Figure 6.7 showing the testing results of the proposed error correction algorithm. The distance for testing translation error compensation was 254 cm. Results of compensation for translation error is given in Figure6.3.

The square path for testing orientation error compensation was 254 cm $\times$ 254 cm as shown in Figure 6.4. Figure 6.5 $\sim$ Figure 6.7 are results of both clockwise and counter-clockwise testings.

From the testing results, localization errors were greatly reduced. This proved the effectiveness of the compensation algorithms. The compensation algorithms are

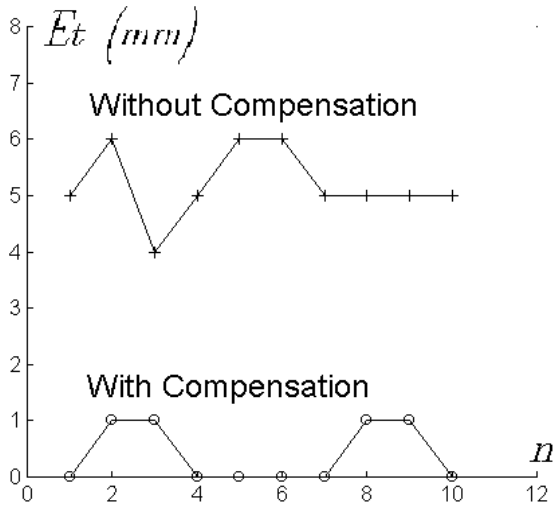

Figure 6.3: Translation error compensation. n is the time sequence. o is the error without error compensation and + is the corresponding error with error compensation.

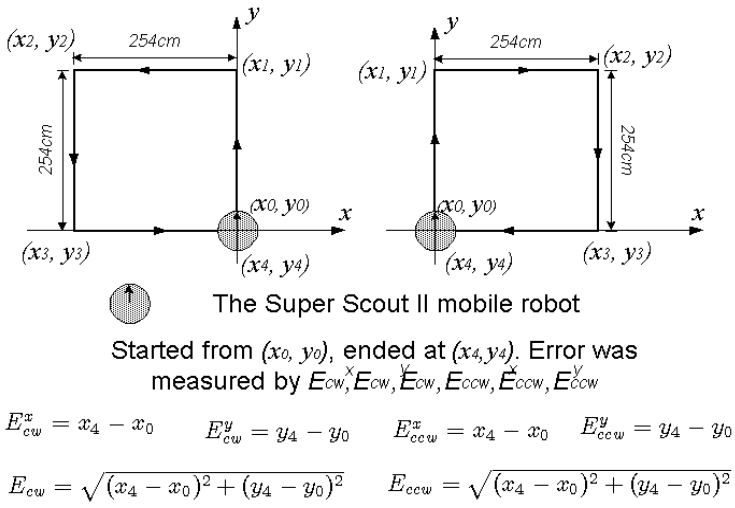

Figure 6.4: Orientation error compensation. Error in x position. a. Clockwise rotation. b. Counter-clockwise rotation.

working continuously during the navigation. After the error compensation has been applied, errors in the positional information from dead reckoning are then reduced to a tolerable level that was sufficient for the purpose.Therefore now dead reckoning technique can be used for localization purpose. Using these results, a simple path

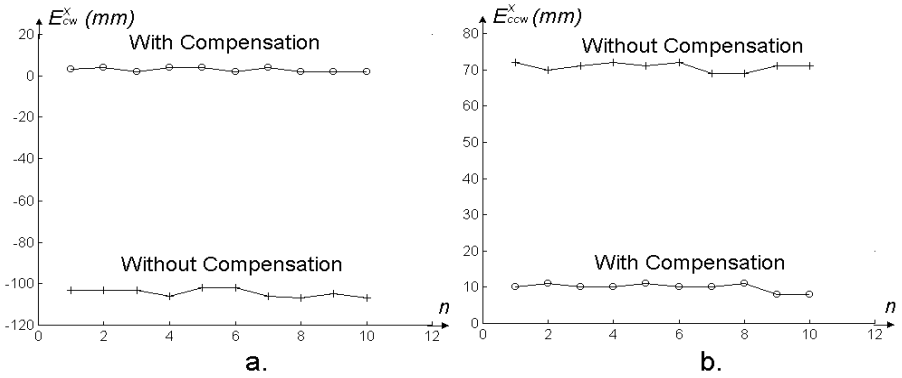

Figure 6.5: E^x_{cw} is the clockwise rotation error in x coordinate. E^x_{ccw} is the counter-clockwise rotation error in x coordinate. n is the time sequence. o is the error without error compensation and + is the corresponding error with error compensation.

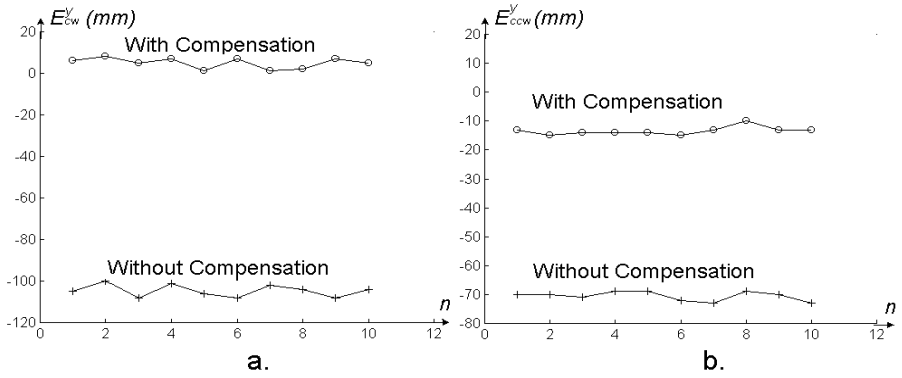

Figure 6.6: E^y_{cw} is the clockwise rotation error in y coordinate. E^y_{ccw} is the counter-clockwise rotation error in y coordinate. n is the time sequence. o is the error without error compensation and + is the corresponding error with error compensation.

planning strategy was developed based on the map produced.

6.2 Path Planning for Autonomous Navigation

A mobile service robot is designed to perform certain tasks. The path planning strategy is based on the target that the robot should be able to complete such tasks [88, 75]. In our project, the path planning strategy has been focused on the

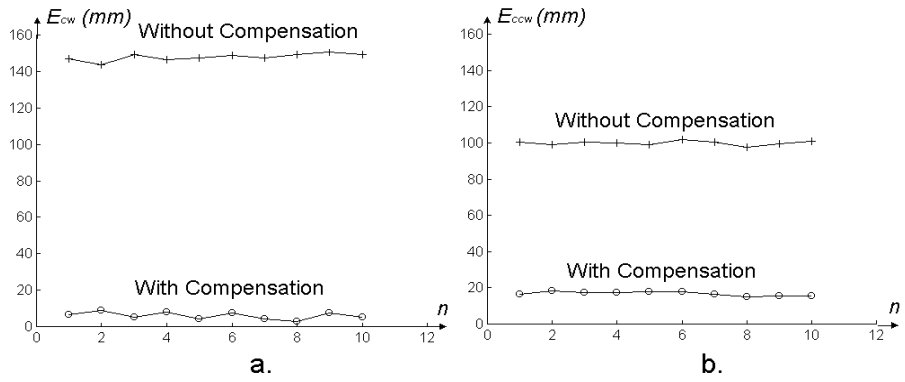

Figure 6.7: E_{cw} is the clockwise rotation error. E_{ccw} is the counter-clockwise rotation error. n is the time sequence. o is the error without error compensation and $+$ is the corresponding error with error compensation.

aim that the robot is to clean the free space in its surroundings. A simple path planning strategy has been derived to meet this requirement. Figure 6.8 shows the process of this strategy. The strategy is aimed to make the robot navigate through

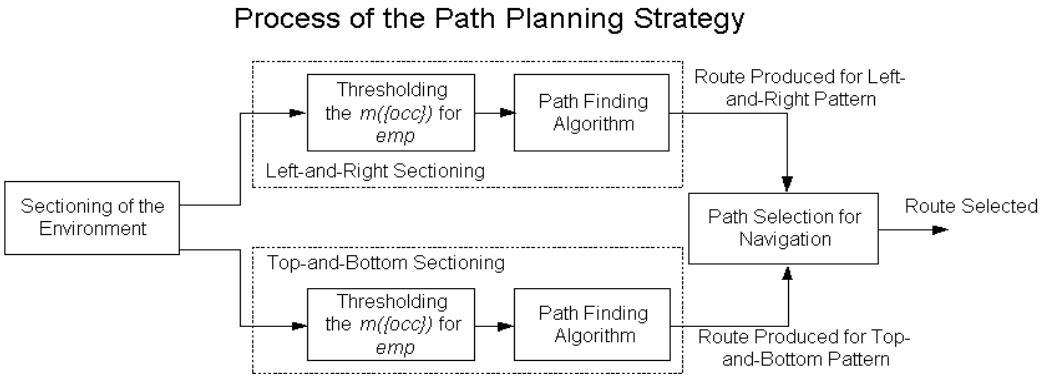

Figure 6.8: Diagram of the path planning process.

free space from the grid map produced. The path finding algorithm makes use of the evidence of being *empty* of each cell in the grid map. Two patterns of paths are proposed of which the one that covers more cells is selected as the route to be followed by the robot. The path following is then carried out using dead reckoning for self-localization.

The path planning strategy was developed mainly based on two considerations.

One is that the map building strategy is grid-based evidence method. The path planning strategy has to be working under the environmental information reflected by the map. The other is due to the purpose of the navigation. For a service robot used in a confined space, we expect it to be able to cover all free areas in the environment to perform tasks such as cleaning the floor.

With no *a priori* environmental knowledge, the robot does not know how big the surrounding environment is, therefore the exact number of how many cells should be covered is unavailable when the navigation starts. When the grid map has been generated, with evidence values attached to every cell, the path planning strategy is able to find those cells that can be traveled safely by the robot in the current grid map. Since each cell on the grids represents an small square area in the actual environment with fixed size, the number of cells that can be marked for navigation according to the evidence attached to that cell is then the problem of interest for path planning. The path planning strategy proposed here is simple yet effective to satisfy these requirements.

6.2.1 Sectioning of Free Space

After the grid-based map has been produced, the map is sectioned into two patterns, left-and-right pattern and top-and-bottom pattern. The sectioning is based on the position from where the robot is to navigate. Figure 6.9 shows the left-and-right pattern sectioning and Figure 6.10 shows the top-and-bottom pattern sectioning.

The sectioning is based on the current starting position of the robot as there is no *a priori* environmental knowledge for the robot. In either of the two sectioning patterns, the robot is to move in a zigzag way as shown in Figure 6.9 and Figure 6.10. A path finding algorithm will be done on both of the two sectioning patterns.

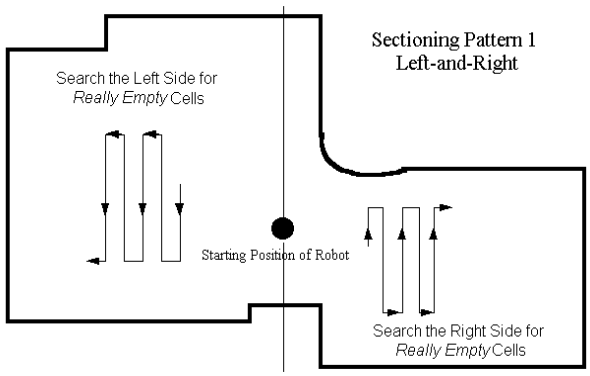

Figure 6.9: Sectioning for path planning: left-and-right pattern.

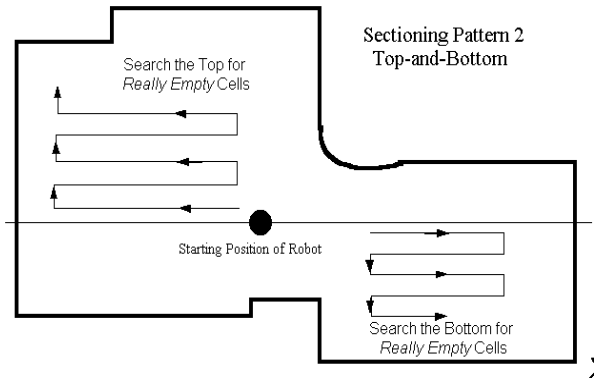

Figure 6.10: Sectioning for path planning: top-and-bottom pattern.

The path finding is done in the two areas one by one for either of the two sectioning patterns. For example, for the left-and-right sectioning pattern as shown in Figure 6.9, path finding is restricted in left side first and then in the right side. For the left side, the route is produced in a down-left-down-left direction and for the right side the route is done is a up-right-up-right direction. The turning points where the route changes its directions are decided by the path finding rule discussed in the next section. The two routes are connected at the starting position of the robot. This produces one complete route in this sectioning pattern which covers the empty area in a zigzag way. There is a similar process for the top-and-bottom sectioning but the zigzag route is left-up-left-up in the top area and right-down-right-down in

the bottom area.

A path finding algorithm is then used to generate safe paths for the two zigzag path patterns. Both of the two paths are guaranteed to be safe to travel by the path finding algorithm. Finally one of the two zigzag paths that covers more area in the grid map will be selected as the one to be used by the robot for performing its task.

6.2.2 The Path Finding Algorithm

A path finding algorithm searches the free space in the map according to the evidence information from $m(\{empty\})$ of each cell. The algorithm first thresholds the $m(\{empty\})$ of each cell as,

$$emp_{i,j} = \begin{cases} 1, & \text{for } m_{i,j}(\{empty\}) \geq T \\ 0, & \text{otherwise} \end{cases} \tag{6.6}$$

where T is a constant defining the desired threshold and $i = 1,\cdots, GridsMapWidth$, $j = 1,\cdots, GridsMapLeng$. $GridsMapLength$ and $GridsMapWidth$ are the maximum length and width of the evidence grids. T has been set to be 0.9. This means only those cells whose $m(\{empty\})$ is over $T = 0.9$ are considered as *really empty* for navigation. The higher the T is, the more conservative this thresholding process is, and accordingly, the fewer *really empty* cells there are. Those cells whose evidence for being *empty* that do not satisfy Equation (6.6) are then discarded in the following path finding process. For the same environment as shown in Figure 5.12, the grid map after the thresholding is given in Figure 6.11.

After the thresholding, the *emp* in each cell is either 1 or 0. A path finding algorithm then searches for paths based on cells' evidence values for being *empty*.

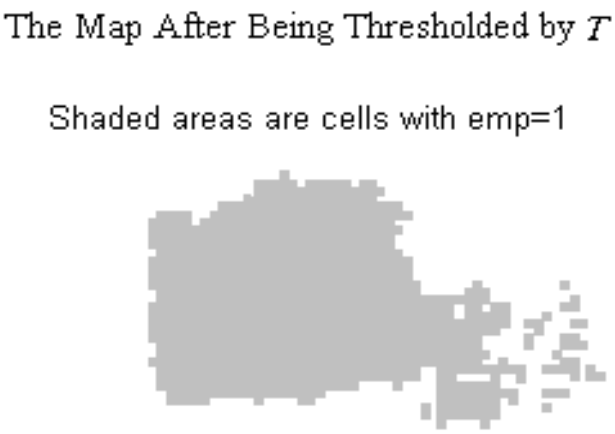

Figure 6.11: Grid map f at T=0.9 for path finding.

The algorithm starts from the current position of the robot. Since the sectioning of the environment has fixed the robot's navigation direction in the zigzag shape, the evidence value on the next cell in this direction will then be checked for its validity of navigation. This process is shown in Figure 6.12 where the robot is to move from position a to position b located at cell (i, j).

$$sum = \sum_{m,n=-2,-1,0,1,2} emp_{i+m,j+n} \tag{6.7}$$

The algorithm uses Equation (6.7) to calculate the sum of $emp_{i,j}$ of all 25 grid cells centered at (i, j). The maximum of sum in Equation (6.7) is 25 as $emp_{i,j}$ is either 1 or 0 after the thresholding. When $sum = 25$, this means all 25 cells surrounding the cell (i, j) are *really empty*. Then the center cell (i, j) is marked as *safe to travel* and registered to be part of the route of the robot. The reason to choose 24 neighboring cells of cell (i, j) is due to the physical dimensions of the robot. The Nomad Super Scout II is 41cm in diameter and the grid cell is 10cm by

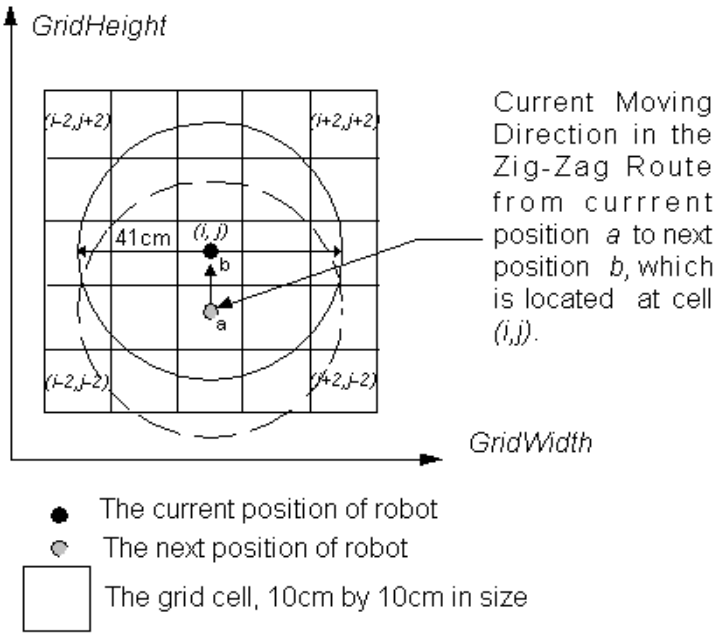

Figure 6.12: Calculating the sum of *emp* of 25 cells centered at cell(i, j) in path finding. The robot whose center is located at cell(i, j) is completely covered by the 25 cells.

10cm. As shown in Figure 6.12, the area occupied by the robot is completely inside the area covered by the 25 cells.

In this way, every step of the robot is guaranteed to be free of collision by the 25 cells' *emp*=1 as shown in Equation (6.7). This rule is very conservative as for those cells whose $sum < 25$ are discarded as *unsafe to travel* by the robot. How conservative this path finding rule is depends on the threshold value T given by Equation (6.6).

If the cell (i, j) does not satisfy Equation (6.7), the algorithm will check the next cell in the zigzag direction. For example, for the right side in the left-and-right pattern sectioning shown in Figure 6.9, the algorithm checks every along the zigzag path. It starts from the starting position of the robot and move from the bottom to the top in Figure **??**. When the next cell does not satisfy Equation (6.7), the

routes turns left twice to continue moving from the top to the bottom. The route then moves all the way down from the top to the bottom until it reaches the bottom boundary, it then turns right twice to again move from the bottom to the top. The change of direction in the route is thus controlled by Equation (6.7).

Using this algorithm, we can generate safe path patterns as shown in Figure 6.9 and Figure 6.10. A counting process is then done to calculate the number of cells covered in the shaded area for both of the two path patterns. This would ensure that the robot is able to cover as large the area as possible. Figure 6.13 and Figure 6.14 are two routes proposed for the two sectioning patterns. Figure 6.15 gives the overlapped two routes from left-and-right pattern and top-and-bottom pattern. The one with more cells covered is then selected as the preferred route for navigation. In this example, the route selected from Figure 6.13 and Figure 6.14 is shown in Figure 6.16.

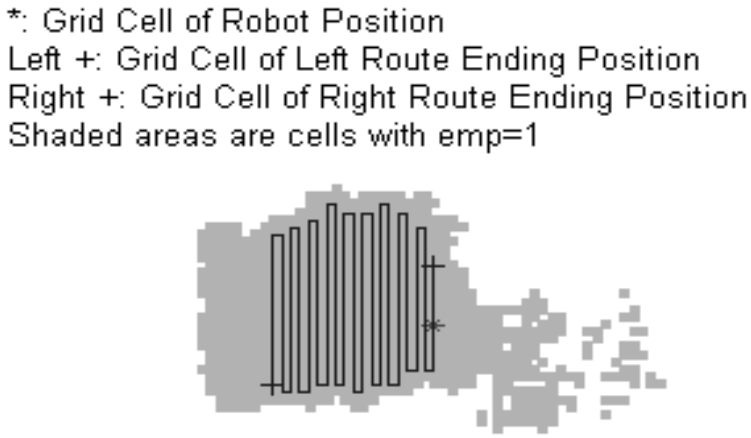

Figure 6.13: The route proposed by the path finding algorithm for left-and-right sectioning.

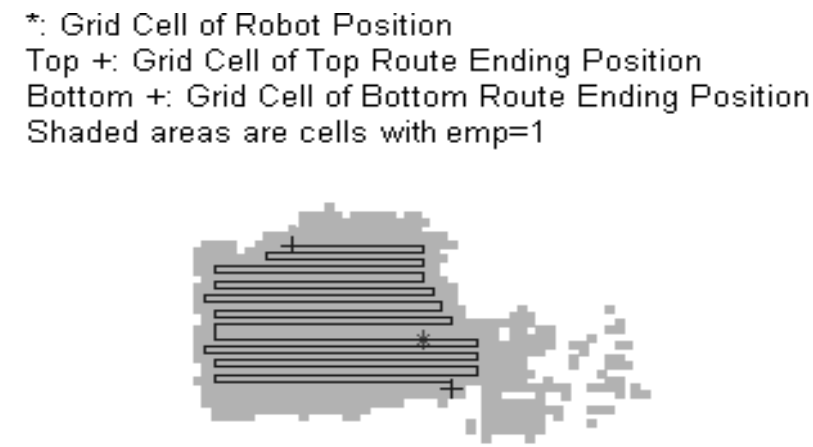

Figure 6.14: The route proposed by the path finding algorithm for top-and-bottom sectioning.

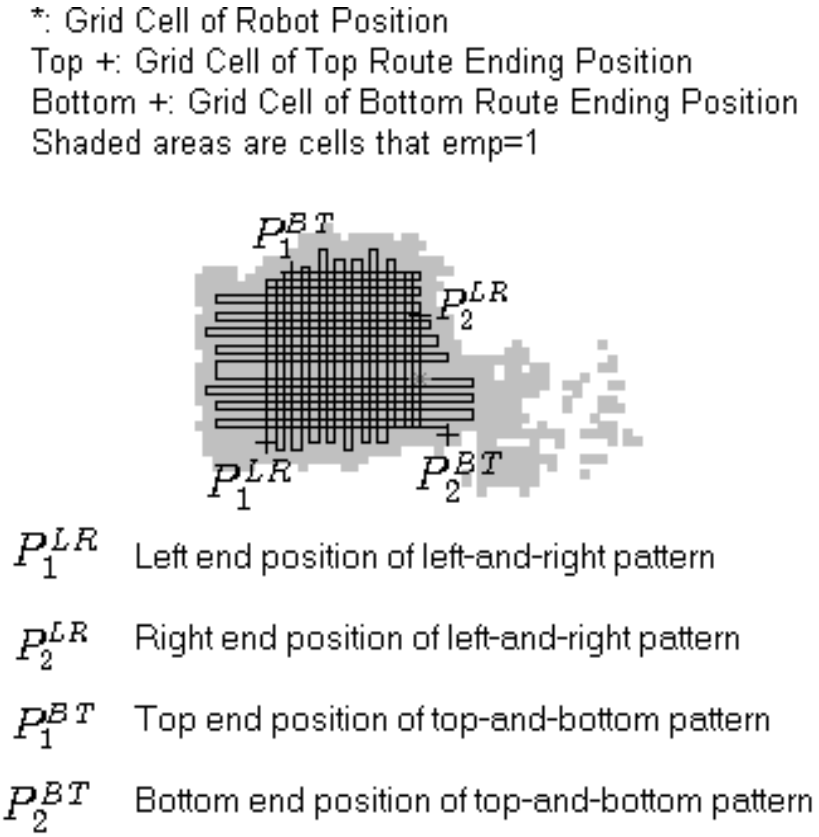

Figure 6.15: The overlapped left-and-right pattern route and top-and-bottom route.

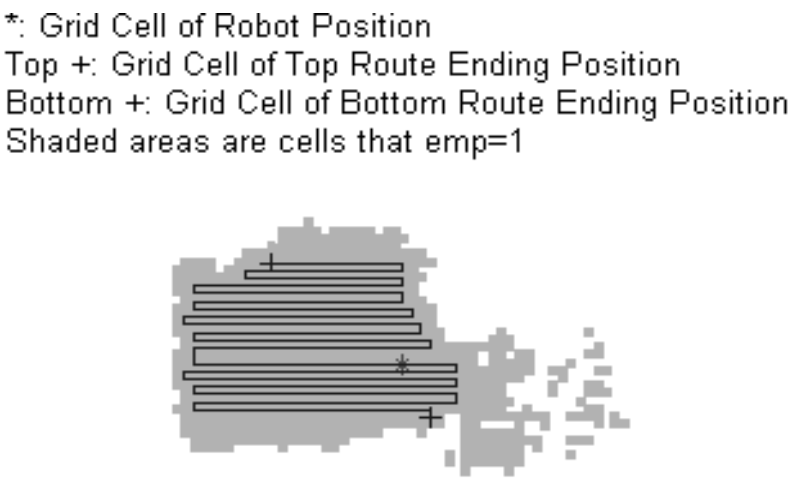

Figure 6.16: The route selected for navigation.

The proposed path planning strategy is very simple and easy to realize. After the path planning, the robot is to follow the selected route to cover free areas in the environment. In next chapter, online experimental results in a testing environment are presented, including the grid map building, multi-ultrasonic sensor fusion and path planning.

Chapter 7

Real-time Experiments

In previous chapters, we have presented experimental results that were calculated off-line based on the data collected in practical confined environments. The mobile robot in those experiments were collecting ultrasonic sensor responses at known positions. In this chapter, the real-time experimental results were presented in a new testing confined space.

7.1 The Mobile Robot Platform

The robot platform used in experiments is a Nomad Super Scout II. The appearance of the robot is given in Figure 7.1. There are 16 Polaroid 600 ultrasonic sensors installed on the robot. As shown in Figure 7.1, the 16 sonars are arranged evenly in a ring with a separating angle of 22.5 degrees. Detailed information can be found in Appendix B. In all experiments, the 16 sonars were fired every 20 ms in sequential order from S_0 to S_{15}.

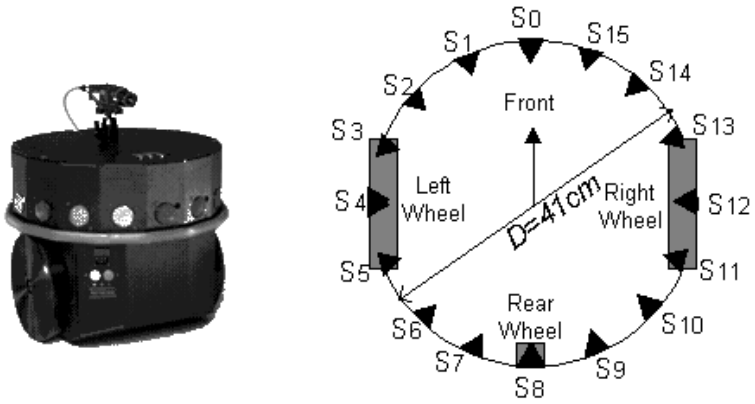

Figure 7.1: The overview of the Nomad Super Scout II mobile robot.

7.2 Experimental Results

7.2.1 Test Environment Setup

The testing environment is given in Figure 7.2.

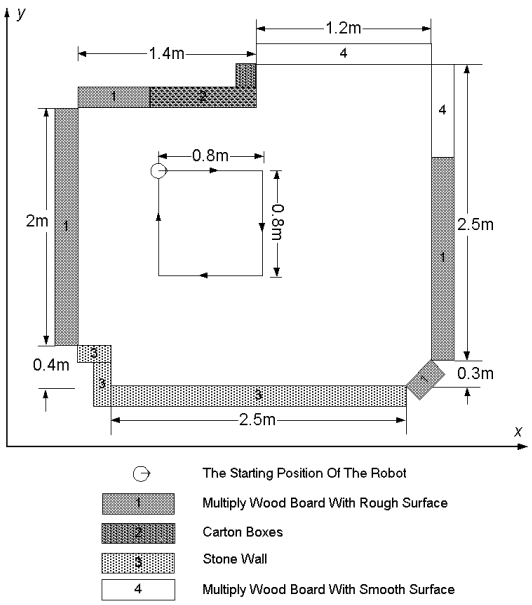

Figure 7.2: The confined test environment.

The Nomad Super Scout II mobile robot was programmed to move in a square path in the clock-wise direction. The size of the square is 0.8m by 0.8m. The starting position of the robot was chosen arbitrarily inside the testing environment.

7.2.2 Experimental Results

Experimental results for the testing confined environment are given in Figure 7.3 $\sim$ Figure 7.11. Among them, Figure 7.3 $\sim$ Figure 7.5 are grid maps produced without the *adaptive sensor model* and the outlier rejection algorithm proposed in this thesis for specular reflections, Figure 7.6 $\sim$ Figure 7.8 are grid maps produced with the *adaptive sensor model* and the outlier rejection algorithm, and Figure 7.9 $\sim$ Figure 7.11 are results of the path planning algorithm.

The robot was continuously updating the grid map during the experiment. Figure 7.3 $\sim$ Figure 7.5 are grid maps produced in 3 sampling positions after different rounds of sonar ring scans.

The testing confined environment is quite specular reflective. Without our proposed methods, the robot was not able to cancel unreliable readings as typically shown in Figure 7.5. Figure 7.6 $\sim$ Figure 7.8 are grid map building results after the adaptive sensor model and the ORA have been applied.

From Figure 7.6 $\sim$ Figure 7.8, unreliable sensor responses have been successfully reduced as compared with corresponding figures in Figure 7.3 $\sim$ Figure 7.5. These real-time experimental results together with previous simulation results have proved the effectiveness of the adaptive sensor model and the ORA. Comparing with Figure 7.3 and Figure 7.6, we also notice that the proposed methods caused

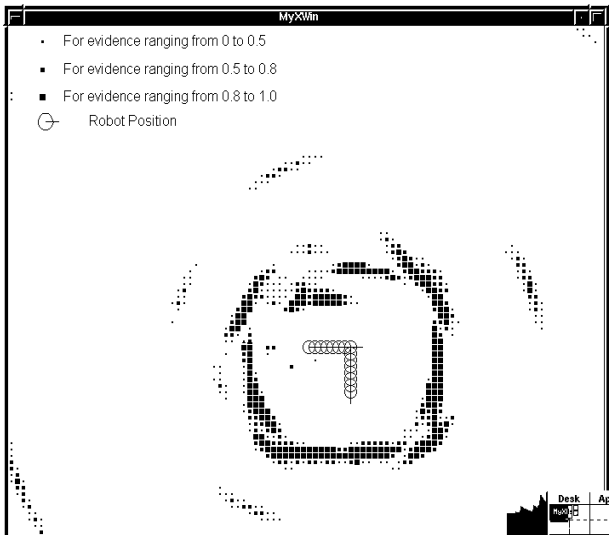

Figure 7.3: Grid map for being *occupied* without adaptive sensor model and outlier rejection algorithm after 16 sonar scans.

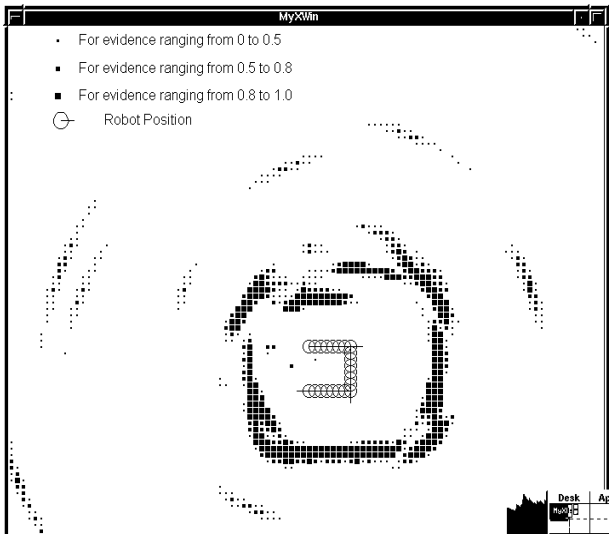

Figure 7.4: Grid map for being *occupied* without adaptive sensor model and outlier rejection algorithm after 24 sonar scans.

some information loss. However, after 32 rounds of sonar ring scans, the information in the grid map produced in Figure 7.8 was sufficient. Figure 7.8 has improved the

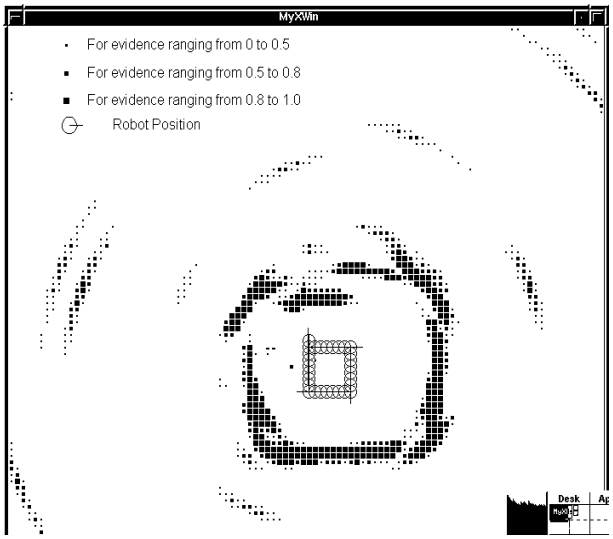

Figure 7.5: Grid map for being *occupied* without adaptive sensor model and outlier rejection algorithm after 32 sonar scans.

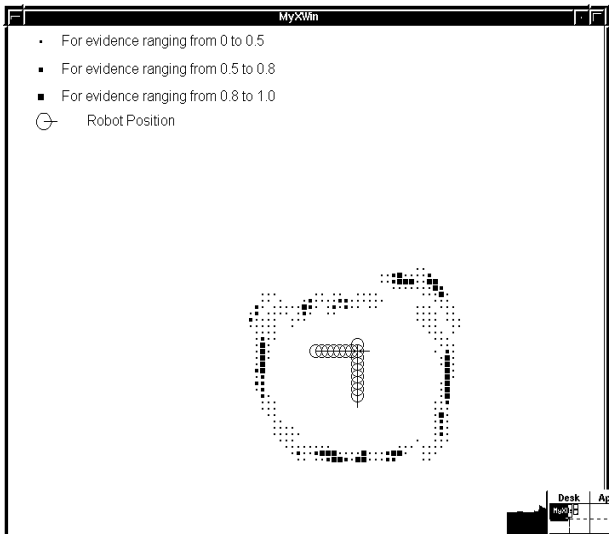

Figure 7.6: Grid map for being *occupied* with adaptive sensor model and outlier rejection algorithm after 16 sonar scans

accuracy of the grid map produced.

The path planning strategy began the processing on the produced grid map after

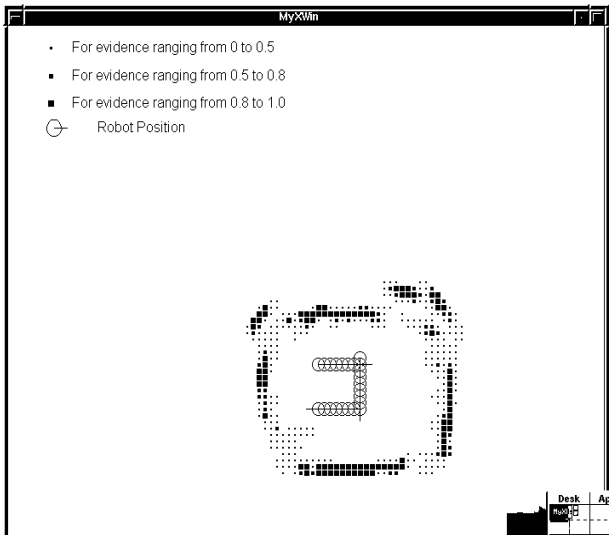

Figure 7.7: Grid map for being *occupied* with adaptive sensor model and outlier rejection algorithm after 24 Sonar Scans

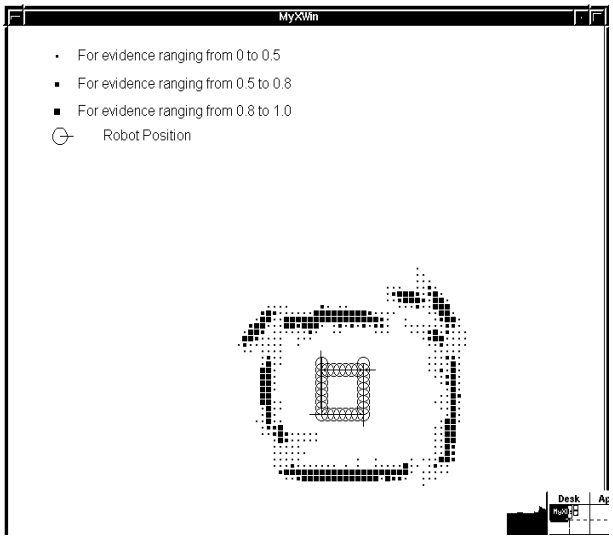

Figure 7.8: Grid map for being *occupied* with adaptive sensor model and outlier rejection algorithm after 32 sonar scans

the map building process. The path planning strategy produced the path for each sectioning pattern as shown in Figure 7.9 and Figure 7.10.

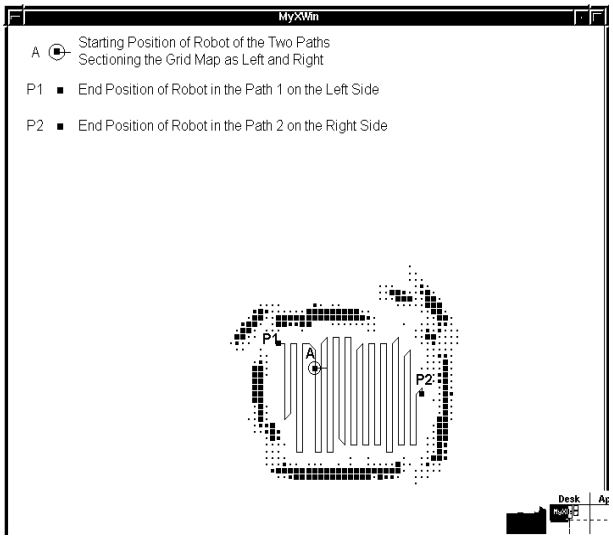

Figure 7.9: Route produced in left-and-right pattern sectioning in testing confined environment.

The path planning strategy selected the preferred route which covered more free space as shown in Figure 7.11. From the route selected by the path planning strategy, in the premise that the robot is free of collision, the route covers most of the free space in the previously unknown environment. Therefore the robot is able to clean most of the floor of this testing environment.

The experimental results were successfully good enough to say that the proposed approach of using adaptive sensor model with modified *RCF* and *ORA* could be a workable method in dealing with specular reflections. However, due to inadequate experimental results, what we have obtained so far is more a preliminary investigation than a complete proof, which needs much more effort on testing it completely

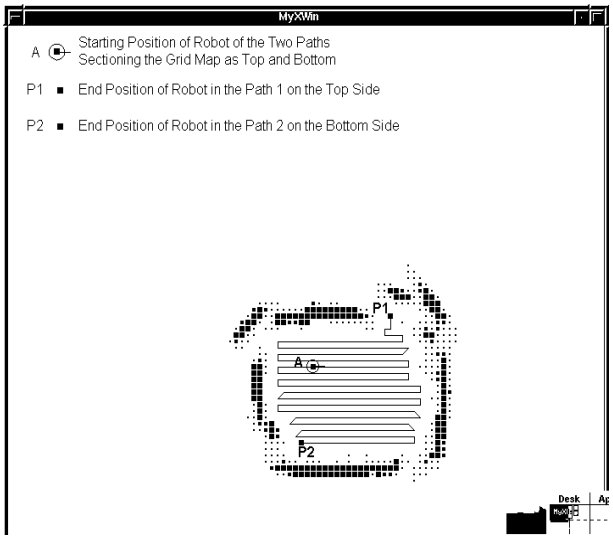

Figure 7.10: Route produced in top-and-bottom pattern sectioning in the testing confined environment.

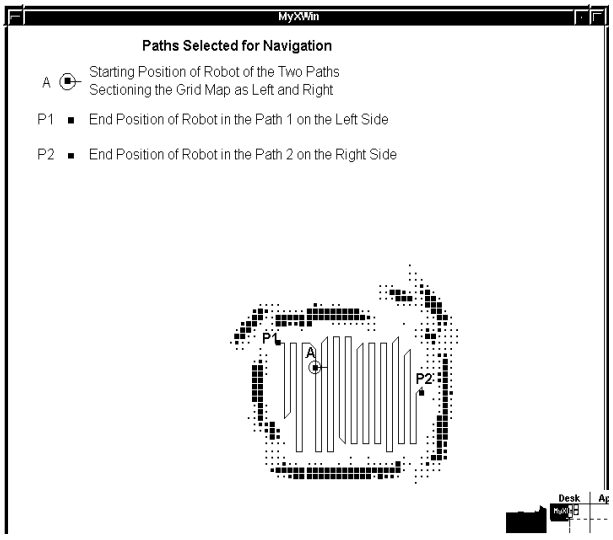

Figure 7.11: Path selected for navigation in the testing confined environment.

in all possible cases of surrounding environments, such as the environment with a variety of reflecting materials, the environment with more obstacles inside

Chapter 8

Conclusions and Recommendation

8.1 Conclusions

In this thesis, the multi-ultrasonic sensor fusion for a mobile robot in confined environments has been investigated. Grid-based map building has been implemented with fused multi-sensory information. Due to the specular reflections that cause unreliable sensor responses, special efforts have been made on proposing new methods to deal with specular reflections. With the improved map, path planning strategy produces the route for the robot to perform the floor cleaning in the free space of its surroundings.

With both off-line calculation and real-time experimental results presented in previous chapters, we have achieved the following:

1. Using Dempster-Shafer's evidence method to integrate the multi-ultrasonic sensory information on the evidence grid has been accomplished to produce the grid-based map for autonomous navigation.

2. The proposed methods of using adaptive sensor model and the outlier rejection algorithm worked well in canceling unreliable ultrasonic sensor readings caused by specular reflections. The new ultrasonic sensor model has improved the accuracy of the grid-based map produced.

3. The error correction algorithms for dead reckoning are able to help the robot perform the self-localization during the navigation.

4. The simple path planning strategy is easy to be realized. The path finding algorithm is useful in searching for empty areas in the grid map produced. The robot is able to follow the path selected which covers most empty areas in the environment.

8.2 Recommendation for Future Work

Through this project we also have noticed that there are still some problems that should receive further attention. Since the idea of using adaptive sensor model with modified RCF and the ORA performed well in our preliminary experimental results, a lot more work is needed to push these preliminary investigation into true experiments. We include here as some recommendation for future work.

1. More experiments in various type of environments, with different specular reflection features are needed. These may include room whose walls are of different characteristics, such as smooth and rough wall, glass or wooden wall. Environments with objects of various specular reflection features inside should be considered. Environments with various geometrical features should also be taken into consideration. For even more complicated case, testings in the

dynamic environment with various of moving objects inside should also be implemented.

2. More efforts are needed in analyzing the experimental data during the multi-ultrasonic sensor fusion process. These analyses may include the change of □ in each grid cell throughout the experiment. Analyses should be made for various testing environments in order to make comparisons on □ among different specular reflection environments. Such analyses may shade further light on the influence of □ on a sensor model.

3. To compute thew match between the evidence grid and the ground truth, a metric should be used. One possibility is the one proposed by Robin R. Murphy, Kevin Gomes and Dave Hershberger [78] as a quantitative metric for expressing the difference in the quality of evidence grids.

4. For a complete robot navigation system, we should not use dead reckoning as the single localization method. Other continuous localization methods should be implemented in our future work. One of the possible methods that can be used is the one proposed by Brian Yamauchi, Alan Schultz, and William Adams [1, 9, 10], which was based on a matching process on the grid map generated from the sonar and other sensory information.

5. The current path planning strategy is simple and it work well in helping us test our sensor model. But how optimal the path generated can be has not been studied in this project. Also, no experiments have been done on the effect of the path planner in various environments or navigation conditions. This part will also receive more attention in our future work.

Author's Publications

- **Published Papers**

  1. **Zou Yi**, Ho Yeong Khing, Chua Chin Seng and Zhou Xiao Wei, "Evidence Method in Ultrasonic Sensor Fusion for Mobile Robots", *Proceedings of the Nineteenth IASTED International Conference on Modeling, Identification and Control*, pp. 7-10, February 2000, Innsbruck, Austria.

  2. **Zou Yi**, Ho Yeong Khing, Chua Chin Seng and Zhou Xiao Wei, "Multi-sensor Fusion for Autonomous Mobile Robots, *Proceedings of SPIE in Sensor Fusion: Architectures, Algorithms, and Applications*, Vol. 4051, pp. 314-321, April 2000, Florida, USA.

  3. Zhou Xiao Wei, Ho Yeong Khing, Chua Chin Seng and Wei, **Zou Yi**, "Localization of Mobile Robot Based on Laser Scanner", *Canada Conference on Electrical and Computing and Engineering*, pp. 841-845, May 2000, Nova Scotia, Canada

- **Accepted Papers**

  1. **Zou Yi**, Ho Yeong Khing, Chua Chin Seng and Zhou Xiao Wei, "Multi-ultrasonic Sensor Fusion for Mobile Robots", *IEEE Intelligent Vehicles Symposium*, Octorber 2000, Dearborn, MI, USA

  2. **Zou Yi**, Ho Yeong Khing, Chua Chin Seng and Zhou Xiao Wei, "A New Solution for Specular Reflection in the Multi-ultrasonic Sensor Fusion for Mobile Robots", *IEEE International Conference on Intelligent Robotics and Systems*, November 2000, Takamatsu, Japan

3. Zhou Xiao Wei, Ho Yeong Khing, Chua Chin Seng and **Zou Yi** "Robot Localization in Cluttered Environment Using Laser Scanner", *ICARF 2000, The Sixthe International Conference on Control, Automation, Robotics and Vision*, December 2000, Singapore

Bibliography

[1] Alan C. Schultz and William Adams, "Continuous Localization Using Evidence Grids", *Proceedings of the 1998 IEEE International Conference on Robotics and Automation*, pp.1401-1406, 1998.

[2] Alexander Zelinsky, "A Mobile Robot Exploration Algorithm", *IEEE Transactions on Robotics and Automation*, VOL. 8, NO. 6, 707-717, 1992.

[3] Alberto Elfes "Sonar-Based Real-World Mapping and Navigation",*IEEE Journal of Robotics and Automation*,VOL. RA-3, NO. 3, pp.249-265, 1987.

[4] Alberto Elfes, "Occupancy Grids: A Stochastic Spatial Representation for Active Robot Perception", *Proceedings of the Sixth Conference on Uncertainty in AI*, pp.60-70, July 1990.

[5] Andrew Howard and Les Kitchen, "Generating Sonar Maps in Highly Specular Environments, *Proceedings of the Fourth International Conference on Control, Automation, Robotics and Vision*, pp.1870-1874, 1996.

[6] Belur V. Dasarathy, "Sensor Fusion Potential Exploitation — Innovative Architectures and Illustrative Applications", *Proceedings of the IEEE*, VOL. 85. NO.1 pp. 24-38, January 1997.

[7] Billur Barshan and Roman Kuc, "Differentiating Sonar Reflections from Corners and Planes by Employing an Intelligent Sensor", *IEEE Transactions on Pattern Analysis and Machine Intelligence*, VOL. 12, NO. 6, June 1990.

[8] Brisel Ayrulu, Billur Barshan, and Simukai W. Utete, "Target Identification with Multiple Logical Sonars Using Evidential Reasoning and Simple Majority Voting", *Proceedings of the 1997 IEEE International Conference on Robotics and Automation*, pp. 2063-2068, 1997.

[9] Brian Yamauchi, "Mobile Robot Localization in Dynamic Environments Using Dead Reckoning and Evidence Grids", *Proceedings of the 1996 IEEE International Conference on Robotics and Automation*, pp.1401-1406, 1996.

[10] Brian Yamauchi, Alan Schultz, and William Adams, "Mobile Robot Exploration and Map Building with Continuous Localization", *Proceedings of the 1998 IEEE International Conference on Robotics and Automation*, pp.3715-3720, 1998.

[11] B. Sciele and J.L. Crowley, "A Comparison of Position Estimation Techniques Using Occupancy Grids", *Robotics and Autonomous Systems*, VOL. 12, pp.153-171, 1994.

[12] B. S. Y. Rao, H. F. Durrant-Whyte, and J. A. Sheen, "A Fully Decentralized Multi-Sensor System for Tracking and Surveillance", *The International Journal of Robotics Research*, VOL. 12, NO.1, pp. 20-44, February 1993.

[13] Charles C. Chang and Kai-Tai Song, "Ultrasonic Sensor Data Integration and Its Application to Environment Perception", *Journal of Robotic Systems*, pp.663-677, 1996.

[14] Ching-Chin Tsai, "A Localization System of a Mobile Robot by Fusing Dead-Reckoning and Ultrasonic Measurements", *IEEE Transaction on Instrumentation and Measurement*, VOL. 7, NO. 5, pp. 1399-1404, 1998.

[15] Dale Fixsen and Ronald P. S. Mahler, "The Modified Demspter-Shafer Approach to Classification", *IEEE Transaction on Systems, Man, and Cybernetics*, Part A: Systems and Humans, VOL. 27, NO. 1, pp. 96-104, 1997.

[16] Daniel Pagac. Eduardo, M. Nebot, and Hugh Durrant-Whyte, "An Evidential Approach to Map-Building for Autonomous Vehicles", *IEEE Transaction on Robotics and Automation*, VOL. 14, NO.4, pp.623-629, 1998.

[17] David Kortenkamp, R. Peter Bonasso, and Robin Murphy, *Artificial Intelligence and Mobile Robots: Case Studies of Successful Robot Systems*, AAAI Press/The MIT Press, 1998.

[18] David L. Hall, *Mathematical Techniques in Multisensor Data Fusion*, Artech House, 1992.

[19] Dong Woo Cho, "Certainty Grid Representation for Robot Navigation by a Bayesian Method", *ROBOTICA*, VOL. 8,pp.159-165, 1990.

[20] E. G. Araujo and R. A. Grupen, "Feature Detection and Identification Using a Sonar-Array", *Proceedings of the 1998 IEEE International Conference on Robotics and Automation*, pp.1584-1589, 1998.

[21] Eugene Lukacs, *Probability and Mathematical Statistics*, Academic Press, New York and London, 1972.

[22] Frans Voorbraak, "On the Justification of Dempster's Rule of Combination", *Artificial Intelligence*, VOL. 48, pp.171-197, 1991.

[23] Glenn Shafer, *A Mathematical Theory of Evidence*, Princeton University Press, New York, 1976

[24] Giuseppe Oriolo, Giovanni Ulivi, and Marilena Vendittelli, "Real-Time Map Building and Navigation for Autonomous Robots in Unknown Environments", *IEEE Transaction on Systems, Man, and Cybernetics Part B: Cybernetics*, VOL. 28, NO. 3, pp.316-333, 1998.

[25] Gregory D. Hager *Task-Directed Sensor Fusion and Planning, A Computational Approach*, Kluwer Academic Publishers, 1990.

[26] Hans P. Moravec, "Sensor Fusion in Certainty Grids for Mobile Robots", *AI Magazine*, VOL. 9, NO. 2, pp 61-74, 1988.

[27] Hans-Joachim von der Hardt, Didier Wolf , and René Husson, "The Dead Reckoning Localization System of the Wheeled Mobile Robot ROMANE", *Proceedings of the 1996 IEEE/SICE/RSJ International Conference on Multisensor Fusion and Integration for Intelligent Systems*, pp. 603-610, 1996.

[28] Hugh F. Durrrant-Whyte, *Integration, Coordination and Control of Multi-Sensor Robot Systems*, Kluwer Academic Publishers, 1988.

[29] James J. Clark and Alan L. Yuille, *Data Fusion Sensory Information Processing Systems*,Kluwer Academic Publishers, 1990.

[30] James Manyika and Hugh F. Durrrant-Whyte, *Data Fusion and Sensor Management—a decentralized information theoretic approach*, Ellis Horwood Limited, 1994.

[31] Jack Blitz, *Ultrasonics: Methods and Applications*, London Butterworths, 1971.

[32] Jing-Yu Yang and Yong-Ge Wu, "Detection for Mobile Robot Navigation Based on Multisensor Fusion", *Proceedings of SPIE*, VOL. 2591, pp. 182-192, 1995.

[33] Jiwen Guan and David A. Bell, *Evidence Theory and Its Applications, Volume 1*,North-Holland, 1992.

[34] Johann Borenstein, Everett H. R., and Feng L., *Navigating Mobile Robots : systems and techniques*, Wellesley Mass., 1996.

[35] Johann Borenstein, H. R. Everett, and L.Feng, *"Where am I ?" Sensors and Methods For Mobile Robot Positioning*, The University of Michigan, 1996.

[36] Johann Borenstein and Yoram Koren, "Obstacle Avoidance with Ultrasonic Sensors",*IEEE Journal of Robotics and Automation*,VOL. 4, NO. 2, pp.213-218, 1988.

[37] Johann Borenstein and Yoram Koren, "Histogramic-Motion for Mobile Robot Obstacle Avoidance",*IEEE Transactions on Robotics and Automation*,VOL. 7, NO. 4, pp.535-539, 1991.

[38] Johann Borenstein and Yoram Koren, "The Vector Field Histogram—Fast Obstacle Avoidance for Mobile Robots ",*IEEE Transactions on Robotics and Automation*,VOL. 7, NO. 3, pp.278-288, 1991.

[39] Johann Borenstein and Yoram Koren, "Error Eliminating Rapid Ultrasonic Firing for Mobile Robot Obstacle Avoidance",*Proceedings of IEEE International Conference on Robotics and Automation*, May 1992.

[40] Johann Borenstein and L. Feng, "UMBmark-A Method for Measuring, Comparing, and Correcting Dead-Reckoning Errors in Mobile Robots",*Technical Report UM-MEAM-94-22*, University of Michigan, 1994.

[41] John Hwan Lim and Dong Woo Cho "Experimental Investigation of Mapping and Navigation Based on Certainty Grids Using Sonar sensors", *ROBOTICA* VOL. 11, pp.7-17, 1992.

[42] John Hwan Lim and Dong Woo Cho "Specular Reflection Probability in the Certainty Grid Representation", *Transactions of the ASME*, VOL. 116, pp.512-520, 1994.

[43] John J. Leonard and Hugh F. Durrrant-Whyte,*Directed Sonar Sensing for Mobile Robot Navigation*, Kluwer Academic Publishers, 1992.

[44] J. L. Dáz de León S. and J. H. Sossa A., "Automatic Path Planning for a Mobile Robot Among Obstacles of Arbitrary Shape", *IEEE Transactions on Systems, Man, and Cybernetics—Part B: Cybernetics*, VOL. 28, NO. 3, pp. 467-472, 1998.

[45] Joseph M. Covino and Barry E. Griffiths, "A New Estimation Architecture for Multisensor Data Fusion", SPIE Sensors and Sensor Systems for Guidance and Navigation,VOL. 1478 ,pp.114-125, 1991

[46] Ken Hughes and Robin Murphy, "Ultrasonic Robot Localization Using Dempster-Shafer Theory", *Proceedings of SPIE on Neural and Stochastic Methods in Image and Signal Processing*, VOL. 1766, pp.2-11, 1992.

[47] Kevin Graves, William Adams, and Alan Schultz, "Continuous Localization in Changing Environments, *Proceedings of the 1997 IEEE International Symposium on Computational Intelligence in Robotics and Automation*, pp. 28 -33, 1997.

[48] K. J. Kyriakopoulos and A. Curran, "Sensor-Based Self-Localization for Wheeled Mobile Robots", *Journal of Robots & Systems*, VOL. 12, NO. 3, pp.163-176, 1993.

[49] K. J. Kyriakopoulos and A. Curran, "Ultrasonic Navigation for a Wheeled Nonholonomic Vehicle", *Journal of Intelligent and Robotic Systems*, VOL. 12, NO. 3, pp.239-258, 1995.

[50] K. J. Kyriakopoulos and G. C. Anousaki, "Simultaneous Localization and Map Building for Mobile Robot Navigation, *IEEE Robotics & Automation Magazine*, pp.42-53, September 1999.

[51] Kok Seng Chong and Lindsay Kleeman, "Sonar Based Map Building for a Mobile Robot", *Proceedings of the 1997 IEEE International Conference on Robotics and Automation*, pp. 1700-1705, 1997.

[52] Kulich, M., Stepan, P., and Preucil, L. , "Feature Detection and Map Building Using Ranging Sensors ", *Proceedings of 1999 IEEE/IEEJ/JSAI International Conference on Intelligent Transportation Systems*, pp. 201 -206, 1999,

[53] Larry Matthies and Alberto Elfes,"Integration of Sonar and Stereo Range Data Using a Grid-Based Representation", *IEEE Journal of Robotics and Automation*, pp.727-737, 1988.

[54] Lawrence A. Klein, *Sensor and Data Fusion Concepts and Applications*, VOL. TT 14, SPIE Optical Engineering Press, 1993.

[55] Leopoldo Jetto, Sauro Longhi, and Giuseppe Venturini, "Development and Experimental Validation of an Adaptive Extended Kalman Filter for the Localization of Mobile Robots", *IEEE Transaction on Robotics and Automation*, VOL. 15, NO. 2, pp. 219-229 April 1999.

[56] Leyla Cahut, Kimon P. Valavanis, and Hakan Deliç, "Sonar Resolution-Based Environment Mapping", *Proceedings of the 1998 IEEE International Conference on Robotics and Automation*, pp. 2541-2547, 1998.

[57] Linas J. and Waltz E., *Multisensor Data Fusion*, Artech House, 1992.

[58] Martin Beckerman and E. M. Oblow, "Treatment of Systematic Errors in the Processing of Wide-Angle Sonar Sensor Data for Robotic Navigation",*IEEE Transactions on Robotics and Automation*, VOL. 6, NO.2, pp.137-145, 1990.

[59] Martin C. Martin and Hans P. Moravec, "Robot Evidence Grids", Carnegie Mellon University, 1996.

[60] Michael Drumheller, "Mobile Robot Localization Using Sonar", *IEEE Transactions on Pattern Analysis and Machine Intelligence*, VOL. PAMI-9,NO.2, pp.325-332, 1987.

[61] Mongi A. Abidi and Ralph C. Gonzalez., *Data Fusion in Robotics and Machine Intelligence*, Boston, Academic Press, 1992.

[62] Moshe Kam, XiaoXun Zhu, and Paul Kalata, "Sensor Fusion for Mobile Robot Navigation", *Proceedings of The IEEE*, VOL. 85, NO.1, pp.108-119, 1997.

[63] M. K. Brown, "Feature Extraction Techniques for Recognizing Solid Objects with An Ultrasonic Range Sensor", *IEEE Journal of Robotics and Automation*, RA-1(4), pp.191-205, December, 1985.

[64] Nomad Robotics Company,"Super Scout II Manual", *Nomad Robotics Company*, 1998.

[65] Pei Wang, "A Defect in Dempster-Shafer Theory", *Proceedings of the 10th Conference of Uncertainty in Artificial Intelligence*, Seattle, WA, U.S.A., 1994.

[66] Phil Greenway and Rob Deaves, "Sensor Management Using the Decentralized Kalman Filter",*SPIE Sensor Fusion VII*, VOL. 2355, pp.216-225, 1994.

[67] Polaroid, "Ultrasonic Ranging System", 1987.

[68] Polaroid, "Ultrasonic Ranging System Handbook Application Notes/Technical Papers" , 1987.

[69] Polaroid,"6500 Series Ranging Module", 1998.

[70] C. Biber, S. Ellin, E. Shenk, and J. Stempeck, "The Polaroid Ultrasonic Ranging System", *Presented at the 67th AES Convention*, 1980.

[71] Steve Ciarcia, "Home In on the Range! An Ultrasonic Ranging System", *BYTE Magazine*, 1980.

[72] Raschke U. and Johann Borenstein, "A Comparison of Grid-type Map-building Techniques by Index of Performance",*Proceedings of IEEE International Conference on Robotics and Automation,*,VOL. 3, pp. 1828-1832, 1990.

[73] R. C. Fryxell, "Navigation Planning Using Quatrees", *SPIE Mobile Robots II*, Cambidge, MA, pp. 256-261, November, 1987.

[74] Richard R. Brooks and S. S. Iyengar, *Multi-Sensor Fusion: Fundamentals and Applications with Software*,Prentice Hall, 1997.

[75] Richard R. Brooks, "Solving the Find-path Problem by A Good Representation of Free Space", *IEEE Transaction on Systems, Man, and Cybernetics*, VOL. SMC-13, NO. 3, pp.190-197, 1983.

[76] Rob Deaves and Phil Greenway, "An Experimental Evaluation of Distributed Identity Fusion", *SPIE Sensor Fusion VII*, VOL. 2355, pp.74-83, 1994.

[77] Robert J. Safranek, Susan Gottschlich, and Avinash C. Kak, "Evidence Accumulation Using Binary Frames of Discernment for Verification Vision", *IEEE Transactions on Robotics and Automation*, VOL. 6, NO.4, 1990.

[78] Robin R. Murphy, Kevin Gomes, and Dave Hershberger," Ultrasonic Data Fusion as a Function of Robot Velocity", *Proceedings of SPIE*, VOL. 2905, pp.114-126, 1996.

[79] Robin R. Murphy, "Dempster-Shafer Theory for Sensor Fusion in Autonomous Mobile Robots", *IEEE Transactions on Robotics and Automation*, Vol.14, NO.2,pp.197-206, 1998.

[80] Robin R. Murphy, "Adaptive Rule of Combination for Observations Over Time", *1996 Multisensor Fusion and Integration for Intelligent Systems (MFI96)*, pp.125-131, 1996.

[81] Roman Kuc and Billur Barshan, "A Spatial Sampling Criterion for Sonar Obstacle Detection", *IEEE Transaction on Pattern Analysis and Machine Intelligence*, PAMI-12(7), pp.686-690, 1989.

[82] Roman Kuc and Billur Barshan, "Navigation Vehicles Through An Unstructured Environment With Sonar", *IEEE Journal of Robotics and Automation*,pp.1422-1426, 1989.

[83] Roman Kuc and M. W. Siegel, "Physically Based Simulation Model for Acoustic Sensor Robot Navigation", *IEEE Transactions on Pattern Analysis and Machine Intelligence*,PAMI-9(6), pp.766-778, 1987.

[84] Sherman Y. T. Lang, Larry W. Korba, and Andrew K. C. Wong, "Characterizing and Modeling a Sonar Ring", it SPIE Mobile Robots IV, VOL. 1195, pp. 291-304, 1989.

[85] S. James Press, *Bayesian Statistics: Principles, Models, and Applications*, John Wiley & Sons, New York, 1989.

[86] S. Kambhampati and L. S. Davis, "Multiresolution Path Planning for Mobile Robot", *IEEE Journal of Robotics and Automation*, VOL. RA-2, NO. 3, pp.135-145, 1986.

[87] Sim Hor Peng and Hia Hwee Hoon, *Navigation and Control of A Mobile Robot (II), Final Year Project Report, (C4030)*, Nanyang Technological University, 2000.

[88] S. V. N. Rao, S. S. Iyengar, C. C. Jorgensen and C. R. Weisbin, "Robot Navigation in An Unexplored Terrain", *Journal of Robotic Systems*, VOL. 3, NO. 4, pp.389-407, 1986.

[89] T. Lozano-Perez and M. A. Wesley, "An Algorithm for Planning Collision Free Paths Among Polyhedral Obstacles", *Communication of the ACM*, VOL. 22, NO. 10, pp.560-570, 1979.

[90] Thomas C. Henderson, Mohammed Dekhil, Larry Schenkat,Larkin Veigel, and Beat Bruderlin, "Flat Surface Reconstruction Using Sonar", *The International Journal of Robotics Research*, VOL. 17, NO.5, pp.504-511, 1998.

[91] W. D. Recken, "Concurrent Localization and Map Building for Mobile Robots Using Ultrasonic Sensors", *Proceedings of the 1993 IEEE/RSJ International Conference on Intelligent Robots and Systems*, pp.2192-2197, 1993.

[92] W. D. Recken, "Autonomous Sonar Navigation in Indoor, Unknown and Unstructured Environments", *Proceedings of the 1994 IEEE/RSJ/GI International Conference on Intelligent Robots and Systems*, pp.431-438, 1994.

[93] Zou Yi, Ho Yeong Khing, Chua Chin Seng, and Zhou Xiao Wei, "Evidence Method in Ultrasonic Sensor Fusion for Mobile Robots",*Proceedings of the Nineteenth IASTED International Conference on Modeling. Identification and Control*, pp. 7-10, 2000.

[94] Zou Yi, Ho Yeong Khing, Chua Chin Seng, and Zhou Xiao Wei, "Multi-ultrasonic Sensor Fusion for Autonomous Mobile Robots, *Proceedings of SPIE in Sensor Fusion: Architectures, Algorithms, and Applications*, VOL. 4051, pp. 314-321, 2000.

[95] Zou Yi, Ho Yeong Khing, Chua Chin Seng, and Zhou Xiao Wei, "Multi-ultrasonic Sensor Fusion for Mobile Robots", *IEEE Intelligent Vehicles Symposium*, Dearborn, Michigan, USA, October 4-5, 2000.*(Accepted).*

[96] Zou Yi, Ho Yeong Khing, Chua Chin Seng, and Zhou Xiao Wei, "A New Solution to Specular Reflections in Multi-ultrasonic Sensor Fusion for Mobile Robots", *IEEE Intelligent Robots and Systems*, Takamatsu, Japan, November 2000.*(Accepted)*

Appendix A

Equations for Sequential Updating Using Bayesian Method

$$P(S_i^{emp}|\{R\}_{k+1}) = \frac{P(R_{k+1}|S_i^{emp}) \cdot P(S_i^{emp}|\{R\}_k)}{P(R_{k+1}|S_i^{occ}) \cdot P(S_i^{occ}|\{R\}_k) + P(R_{k+1}|S_i^{emp}) \cdot P(S_i^{emp}|\{R\}_k)} \tag{A.1}$$

$$P(S_i^{occ}|\{R\}_{k+1}) = \frac{P(R_{k+1}|S_i^{occ}) \cdot P(S_i^{occ}|\{R\}_k)}{P(R_{k+1}|S_i^{occ}) \cdot P(S_i^{occ}|\{R\}_k) + P(R_{k+1}|S_i^{emp}) \cdot P(S_i^{emp}|\{R\}_k)} \tag{A.2}$$

where R_{k+1} is the sensor reading at time $k+1$.

Appendix B

The Nomad Super Scout II Mobile Robot Platform

B.1 Overview

The Nomad Super Scout II^{TM} is an integrated mobile robot system with an onboard industrial PC, ultrasonic and tactile sensing modules and an optional vision system. The control system performs sensor and motor control, as well as communication. At a high level, the Nomad Super Scout II is controlled by a small, industrial PC which is mounted internally.

B.2 On-board Computer System

The high-level processor of this system is a Pentium 200 MHz industrial PC. The high-level processor communicates to the low-level processor through a serial port. The low-level processor of this system is a Motorola MC68332. Additionally, a

TMS320C14 DSP is responsible for high-bandwidth motor control at 2 KHz control rates. The software environment used in the Super Scout II is the Red Hat 5.2. The Nomad Super Scout II can be programmed using the Linux-based Nomadic Software Development Environment.

B.3 Sensor Systems

The Nomad Super Scout II comes standard with odometric sensors, a tactile bumper ring, 16 ultrasonic sensors and an optional vision system. The tactile system uses a ribbon switch enclosed in a energy absorbing neoprene channel. The effective range of ultrasonic sensors is from 15 cm to 650 cm configured as a 8-bit value.

B.4 Specifications

ITEMS	VALUES	COMMENTS
Diameter	41 cm	
Height	35 cm	
Weight	25 kg	With batteries
Speed	1.0 m/sec	
Acceleration	$2\text{m}/s^2$	
Payload	5 kg	
Battery Power	432 watt-hour	Removable
Drive System	2 wheel differential drives	At geometric center
Translation	756 counts/cm	
Rotation	230 counts/degree	

Table B.1: Specifications of Nomad Super Scout II Mobile robot platform.